Energy Advances

ROYAL SOCIETY OF CHEMISTRY

REVIEW ARTICLE

View Article Online
View Journal

Cite this: DOI: 10.1039/d4ya00492b

Semitransparent organic and perovskite photovoltaics for agrivoltaic applications

Souk Y. Kim,†[a] Noura Rayes,†[a] Armen R. Kemanian,[b] Enrique D. Gomez[acd] and Nutifafa Y. Doumon[*ade]

Greenhouse structures offer the ability to control the microclimate, enabling year-round crop cultivation and precision agriculture techniques. To maintain optimal crop growth conditions, substantial energy is required to heat, light, irrigate, and ventilate the interior greenhouse environment. The term Agrivoltaics is coined from integrating agricultural land management with renewable solar energy systems. Most agrivoltaic research applications have focused on studying opaque silicon photovoltaics, with limited exploration of novel semitransparent photovoltaics such as organic or perovskite devices. By incorporating semitransparent photovoltaic systems onto greenhouse rooftops, farms can partially generate electricity from solar energy while utilizing the remaining rooftop light transmission to nurture greenhouse plant growth below. This review explores the principles and properties of semitransparent organic and perovskite photovoltaic technologies and their potential benefits for greenhouse applications. Additionally, we discuss practical case studies to illustrate their integration and efficacy in agrivoltaic systems. We also address key metrics such as average visible transmittance, average photosynthetic transmittance, light utilization efficiency, power conversion efficiency, and their impact on greenhouse energy production. We conclude with an analysis of device challenges, including stability and toxicity issues, limited experimental results of semitransparent photovoltaics in current greenhouse agrivoltaics, and the prospects for integrating semitransparent organic photovoltaics and semitransparent perovskite photovoltaics into agrivoltaic systems.

Received 4th August 2024,
Accepted 7th November 2024

DOI: 10.1039/d4ya00492b

rsc.li/energy-advances

[a] Department of Materials Science and Engineering, The Pennsylvania State University, University Park, PA 16802, USA. E-mail: nzd5349@psu.edu
[b] Department of Plant Science, The Pennsylvania State University, University Park, PA 16802, USA
[c] Department of Chemical Engineering, The Pennsylvania State University, University Park, PA 16802, USA
[d] Materials Research Institute, The Pennsylvania State University, University Park, Pennsylvania 16802, USA
[e] Department of Engineering Science and Mechanics, The Pennsylvania State University, University Park, PA 16802, USA
† These authors contributed equally to the manuscript.

Souk Y. Kim

Souk Y. Kim is a PhD student in the Department of Materials Science and Engineering at The Pennsylvania State University. He earned his B.Eng. degree in 2020 and M.Eng. degree in 2022 from Pukyong National University (PKNU), Republic of Korea. He worked as a research assistant at the Korea Institute of Materials Science (KIMS). His research focuses on the development of renewable energy technologies, particularly organic and perovskite solar cells, with a keen interest in their fundamental mechanisms in device performance and degradation, as well as applications for flexible and large-area modules.

Noura Rayes

Noura Rayes is a PhD candidate in the Department of Materials Science and Engineering at The Pennsylvania State University. She earned her BS degree in Mechanical Engineering in 2022 from the University of Rhode Island with minors in Mathematics, Sustainability, and Environmental Engineering. Her interest in renewable energy physics, humanitarian engineering, and passion for wildlife conservation has led her to currently research organic photovoltaic devices for agrivoltaic applications.

1. Background

Sustainable energy development is crucial for addressing the challenges posed by climate change. The accelerated pace of environmental degradation is primarily attributed to land exploitation to expand agricultural and energy infrastructures needed to support our growing population.[1] Hunter *et al.* predict that a 25–70% increase above current production levels will be necessary by 2050 to meet food demand projections.[2] To sustain this growth rate without exacerbating ecological harm, farmers and engineers must find ways to optimize the efficiency of existing agricultural land. The strain imposed on our natural environment has already contributed to alarming ecological predictions: a 23% loss of wildlife habitat by the end of the century and a 69% decline in biodiversity since 1970.[3–5]

The food, water, and energy nexus pertains to how communities can balance the demand for natural resources to sustain human health and environmental integrity across the world. Agriculture, which accounts for 72% of all freshwater withdrawals and 10.6% of total U.S. emissions since 2021, is at the core of this challenge.[6,7] However, agrivoltaic systems—combining agriculture and solar energy—offer a promising solution for communities to sustainably support these needs. Engineers and farmers must advocate for sustainable agricultural policies to support the research and development of novel precision farming technologies. In this review, we discuss solutions to this grand challenge that utilize the unique properties of innovative photovoltaic technologies.

1.1. Introduction to agrivoltaics

Agrivoltaics describes the integration of photovoltaic (PV) systems with agriculture to optimize land for both energy production and farming practices.[8,9] Agrivoltaic techniques have also been applied in industrial greenhouses to reduce existing energy demands for farmers, thereby promoting economic and environmental sustainability.[9] The primary aim of greenhouses is to maintain a controlled microenvironment favorable to the year-round cultivation of produce. In terms of energy consumption, greenhouses use passive solar to reduce heating costs; however, energy savings can reach up to 80% through further retrofit of conventional design.[10] In particular, electricity for these structures can be generated on-site by partially incorporating PV modules into the rooftop infrastructure, further conserving more land space. Fig. 1a highlights the general principle for land use efficiency of these systems. Fig. 1b is a representative model for semitransparent photovoltaics (ST-PVs) integration with greenhouses, modified from Macknick *et al.*, while Fig. 1c and d demonstrate real-life implementations of this concept.[8,11,12]

Typically, greenhouses are constructed with a metallic framework and covered with durable transparent materials, such as plastic or glass, to protect crops against severe weather conditions.[13] Various designs have been explored for integrating

Armen R. Kemanian

Armen R. Kemanian is a Professor in the Department of Plant Science at The Pennsylvania State University. He obtained his PhD in Engineering Science at Washington State University in 2003. With expertise in modeling, environmental biophysics, plant physiology, and soil biogeochemistry, his research interest attends the interface of food production and the environment, as well as the development of sustainable agroecosystems.

Enrique D. Gomez

Enrique D. Gomez is the Interim Associate Dean for Equity and Inclusion for the College of Engineering at The Pennsylvania State University and a professor of Chemical Engineering and Materials Science and Engineering. He obtained his PhD in Chemical Engineering from the University of California, Berkeley in 2007. His work is focused on connecting the chemical structure of soft materials to functional properties to advance a more sustainable society, with a current emphasis on organic solar cells, water filtration membranes, recyclable composites and battery materials, and natural polymers.

Nutifafa Y. Doumon

Nutifafa Y. Doumon is an assistant professor at The Pennsylvania State University. He is a Virginia S. and Philip L. Walker Jr. professor of Materials Science and Engineering and the Fuels Science Program. Before joining Penn State, he worked as a researcher at the National Renewable Energy Laboratory (NREL) in Golden, Colorado, and INRS-EMT in Varennes, Canada. He holds a PhD in Applied Physics and an MSc in Nanoscience from the University of Groningen, the Netherlands. In 2011, he obtained an MSc degree in Theoretical Physics from AUST-Abuja after a BSc degree in Physics in 2009 from the University of Ghana, Legon. His research interests are organic, polymer, and perovskite photovoltaic and optoelectronic device characterization, stability, and reliability testing.

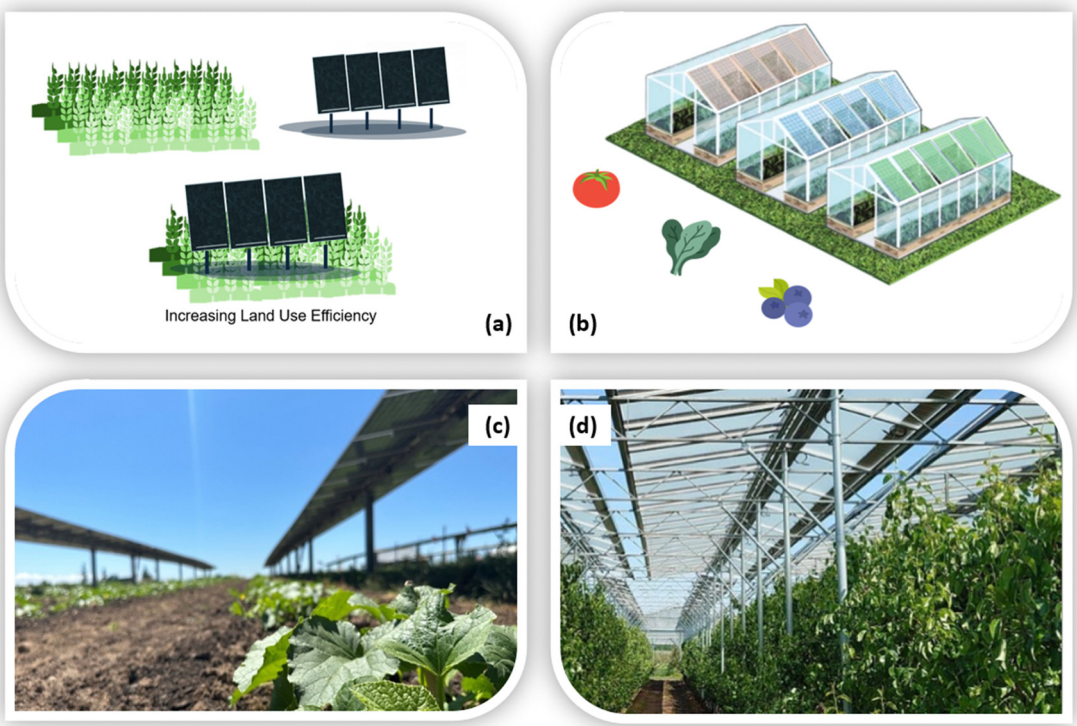

Fig. 1 (a) Visual concept of agrivoltaic dual land use efficiency. (b) The visual concept of semitransparent organic photovoltaics (ST-OPVs) for potential greenhouse applications. Reproduced with permission.[8] Copyright NREL (c) Crops grown under solar panels at Oregon State University. Reproduced with permission.[11] Copyright USDA (d) OPV panels on top of a greenhouse installation at Brite Solar Nanomaterials. Reproduced with permission.[12] Copyright Brite Solar.

PV modules into greenhouses using partial shading and transparency techniques to provide a plant species with the select wavelengths that may be necessary for optimal growth.[14] Luminescent solar concentrators propagate light from the sun *via* a waveguide to photovoltaic cells and have exhibited similar partial shading and energy harvesting properties fitting for these exact systems.[15–18] More ST-PV technologies are increasing in scalability, efficiency, and longevity.[16] Due to their selective light absorption properties and higher efficiencies, ST-PVs are a competitive alternative to standard greenhouse solar energy generation in the future.[14,19]

1.2. Technology principles

Traditional greenhouse agrivoltaics often utilize opaque crystalline silicon and thin-film PVs attached to the roof, which can decrease crop yields due to increased shading.[20] To increase transmission, transparent and translucent photovoltaics have been explored. Transparent devices allow light to pass through them without scattering, while translucent devices refer to semitransparent devices that scatter the incoming light. Organic photovoltaics (OPVs) and perovskite photovoltaics (PPVs) are promising alternatives in solar energy harvesting and agrivoltaic applications because of their semitransparent properties. In principle, PVs convert light into electrical energy using semiconducting materials sandwiched between two electrodes. The semiconductor in the photoactive layer is designed with an appropriate energy bandgap to absorb the radiation of the sun with high efficiency. Photons higher in energy than the material's bandgap can be absorbed, creating an electron–hole pair that can then be separated and extracted by the electrodes to generate electricity.[21] Therefore, lower bandgap semiconductor materials may absorb a broader range of solar radiation, which is advantageous for maximizing light absorption at the expense of lower produced voltage and increased recombination losses.

OPVs and PPVs are particularly beneficial in agrivoltaic systems due to their selective energy bandgap, which enables the tunability of light absorption. By adjusting the photoactive molecules in OPVs or the composition of PPVs, these devices can be designed to selectively absorb certain regions of the solar spectrum while transmitting wavelengths necessary for plant growth.[22] Additionally, both OPVs and PPVs can be produced as flexible panels, allowing easy integration into various greenhouse structures. Despite these similarities, OPVs and PPVs differ in several key aspects, particularly regarding their photoactive constituents. OPVs are based on organic photoactive materials, including small molecules and polymers.[20,22–27] These materials offer flexibility in molecular design, enabling a wide range of absorption profiles.[23,24,28,29] PPVs, on the other hand, are composed of perovskite photoactive materials with a unique crystal structure characterized by the formula ABX_3, where A is a cation (*e.g.*, methylammonium, formamidinium), B is a metal cation (*e.g.*, lead, tin), and X is a halide anion (*e.g.*, iodide, bromide). This versatility in composition contributes to the PPVs' capture of solar energy with high efficiency.[30] The detailed properties and applications of these technologies will be discussed in the following sections.

Research efforts have recently pushed efficiencies at 20% for OPVs[31–33] and over 26% for PPVs.[34,35] The rapid enhancement of their efficiencies makes OPVs and PPVs with absorption tunability and semi-transparency increasingly attractive for integration into agricultural applications. Additionally, the relative ease and low cost of manufacturing these materials further emphasize their potential for widespread use in agrivoltaics. While studies and review papers discuss semitransparent OPVs and PPVs,[26,27,36–39] a comprehensive discussion focusing on their applications in agrivoltaics is still key to their advancement. The review examines the progress, challenges, and future of ST-OPVs and ST-PPVs for agrivoltaic applications. We seek to highlight the potential of the latest research and technological breakthroughs to ensure a sustainable agricultural future where energy generation and food production can coexist in synergy.

2. Special requirements

In agrivoltaics, evaluating the compatibility of ST-PVs alongside agricultural productivity is important in determining the land-use efficiency of the entire system. Therefore, understanding a comprehensive set of figures and metrics from these disciplines is essential to effectively quantifying the relationship between ST-PV and crop yield. The foundation of this work relies on the sun's radiation at Earth's terrestrial surface. After passing through the atmosphere, the total radiation consists of roughly 5% UV, 43% visible, and 52% infrared radiation.[40] On clear days in the summer, the incoming irradiance at noon at sea level is approximately 1000 W m^{-2}. Fig. 2a illustrates the radiation emitted from the sun in W m^{-2} nm^{-1} from 0 to 4000 nm, illustrating the solar irradiance spectra at Earth's atmosphere (AM0) and Earth's surface (AM1.5), respectively. Fig. 2b depicts which wavelengths of light various bodies, including chlorophyll, phytochromes, and many other plant pigments, will absorb for spectral reference. Solar energy harvesting devices are designed to maximize the energy they can produce through the absorption of solar radiation. Thus, Fig. 2c shows a typical absorption profile for ST-OPVs for the AM 1.5G solar emission for a potential agrivoltaic system, *i.e.*, ST-PVs mostly absorb in the UV and NIR while remaining transparent in the visible.

Sunlight absorption in plants is necessary for photosynthesis, in which plants utilize light to store chemical energy.[43] However, under full sun, most of the energy absorbed by the leaves is dissipated as latent and sensible heat and thermal radiation. Near-infrared is not used for photosynthesis. Similarly, plants reflect most green light and thus present a gap in the visible absorption spectrum in the green. Selective wavelength transmission through the device must be considered when pairing the necessary PV with the desired crop to maximize production yields. Visible light is 43% of the total irradiance at Earth's surface, divided into blue light (400–500 nm), green light (500–600 nm), and red light (600–700 nm).[41,44] The light absorption spectrum unique to each plant species is known as photosynthetic active radiation, between 400 and 800 nm, shown in Fig. 2. Various pigments, however, such as chlorophyll A and B within the chloroplast, absorb light wavelengths selectively, thus influencing plant development, leaf area expansion, stem length, and flowering rate.[41,45] More physiological research is needed to collect photosynthetic active region data for specific greenhouse crops.

The average visible transmittance (AVT), the visible light able to pass through a device, can be derived by averaging the total light transmittance measured from 400 to 800 nm against the photopic response of the human eye.[46] This metric facilitates comparing device efficiency with light transparency. The light utilization efficiency (LUE = PCE × AVT) can be calculated to further evaluate the performance of ST-PVs.[47] It is worth noting that LUE in this context is different from light use efficiency, which refers to the efficiency of converting absorbed light into biomass. Unlike AVT, which considers how much incident photon flux passes through a panel, Stallknecht *et al.* introduced another metric, the average photosynthetic transmittance, which considers the required wavelengths for the specific plant.[41] The average photosynthetic transmittance (APT) replaces photopic response with the relative quantum efficiency of plants averaged among 22 varieties established by

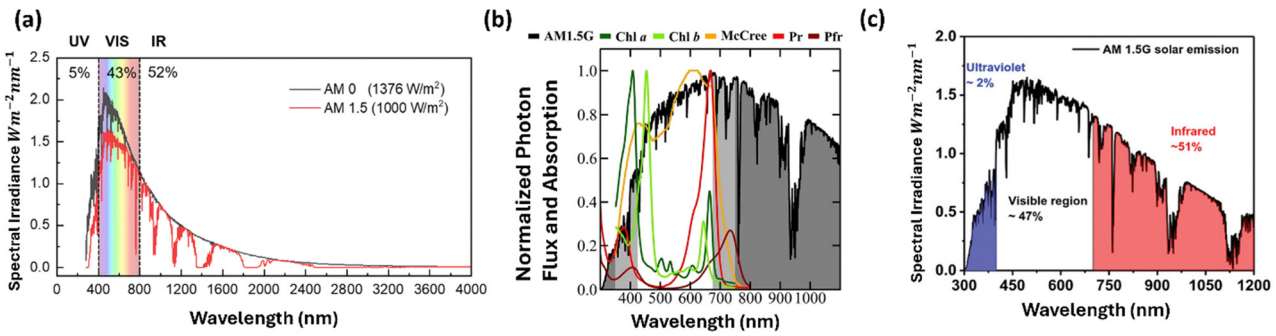

Fig. 2 (a) Solar irradiance spectra (W m^{-2} nm^{-1}) at Earth's atmosphere (AM0) and Earth's surface (AM1.5). The total spectrum is roughly 5% UV, 43% visible, and 52% infrared light. (b) Normalized photon flux and absorption spectra of chlorophyll (Chl) a and b, red-absorbing phytochrome (Pr), far-red-absorbing phytochrome (Pfr), and averaged quantum yield of many plants denoted as McCree. Reproduced with permission.[41] Copyright 2023, Scientific Reports. (c) The absorption spectrum shows the approximate UV and IR regions where an ideal agrivoltaic ST-PV active layer absorbs light, and the visible region is where they can be transparent. Reproduced with permission.[42] Copyright 2021, Wiley-VCH GmbH.

McCree *et al.*[48] The equation for APT is given by the following:

$$\mathrm{APT} = \frac{\int T(\lambda)S(\lambda)P(\lambda)\partial\lambda}{\int S(\lambda)P(\lambda)\partial\lambda},$$

where $S(\lambda)$ is the AM 1.5 photon flux, $T(\lambda)$ is the photon transmittance of the device, and $P(\lambda)$ is the average photosynthetic quantum yield.[41] Plant growth efficiency, quality, and yield are vital agricultural benchmarks, directly correlating the system design and operation with agronomic outcomes. Here, we explore these figures of merit, examining how they are used to balance energy production with agricultural productivity to define the success of agrivoltaics systems.

3. Semitransparent photovoltaics (ST-PVs)

ST-PVs represent a cutting-edge approach to integrating solar energy generation with visual or aesthetic applications, such as building-integrated photovoltaics or agrivoltaics.[47,49,50] These systems strike a balance between optimal light transmission for underlying plant growth and power generation. We explore two prominent types of ST-PVs: semitransparent organic photovoltaics (ST-OPVs) and perovskite photovoltaics (ST-PPVs). Each system has advantages and challenges in terms of efficiency, transparency, and suitability for agrivoltaic systems.

3.1. ST-OPVs

OPVs have several advantages compared to conventional inorganic solar cells.[51,52] OPVs can be lightweight, flexible, and semitransparent, utilizing the conjugated structure of organic donor and acceptor molecules to facilitate electron transfer. Furthermore, OPVs can be fabricated using roll-to-roll or slot-die coating, potentially leading to lower industrial costs and utilizing environmentally benign solution processing.[53,54] However, work is still necessary to improve the efficiency of these devices to match that of inorganic cells. The current efficiency for OPVs has surpassed 20%.[31,32] Nevertheless, this efficiency is not yet on par with that of their inorganic silicon counterpart, which stands at 26.6%.[55,56] OPVs are prone to efficiency losses due to the weak intermolecular coupling and the low dielectric constants of the organic donor and acceptor molecules.[57] The bulk heterojunction morphology is now the most extensively

Table 1 Full name of most organic molecules discussed in the review

P3HT	Poly(3-hexylthiophene-2,5-diyl)
PEDOT:PSS	Poly(3,4-ethylenedioxythiophene)-poly(styrenesulfonate)
$PC_{61}BM$	[6,6]-Phenyl-C61-butyric acid methyl ester
$PC_{71}BM$	[6,6]-Phenyl C71 butyric acid methyl ester
ITIC	3,9-bis(2-methylene-(3-(1,1-dicyanomethylene)-indanone))-5,5,11,11-tetrakis(4-hexylphenyl)
Y6	2,2′-((2*Z*,2′*Z*)-((12,13-bis(2-ethylhexyl)-3,9-diundecyl-12,13-dihydro-[1,2,5]thiadiazolo[3,4-*e*]thieno[2″,3″:4′,5′]thieno[2′,3′:4,5]pyrrolo[3,2-*g*]thieno[2′,3′:4,5]thieno[3,2-*b*]indole-2,10-diyl)bis(methanylylidene))bis(5,6-difluoro-3-oxo-2,3-dihydro-1*H*-indene-2,1-diylidene))dimalononitrile
PM6	Poly[(2,6-(4,8-bis(5-(2-ethylhexyl-3-fluoro)thiophen-2-yl)-benzo[1,2-*b*:4,5-*b*′]dithiophene))-*alt*-(5,5-(1′,3′-di-2-thienyl-5′,7′-bis(2-ethylhexyl)benzo[1′,2′-*c*:4′,5′-*c*′]dithiophene-4,8-dione)]
PBDB-T	Poly[(2,6-(4,8-bis(5-(2-ethylhexyl)thiophen-2-yl)-benzo[1,2-*b*:4,5-*b*′]dithiophene))-*alt*-(5,5-(1′,3′-di-2-thienyl-5′,7′-bis(2-ethylhexyl)benzo[1′,2′-*c*:4′,5′-*c*′]dithiophene-4,8-dione)]
Y6-BO	2,2′-((2*Z*, 2′*Z*)-((12,13-bis(2-butyloctyl)-3,9-diundecyl-12,13-dihydro-[1,2,5]thiadiazolo[3,4-*e*]thieno[2″,3″:4′,5′]thieno[2′,3′:4,5]pyrrolo[3,2-*g*]thieno[2′,3′:4,5]thieno[3,2-*b*]indole-2,10-diyl)bis(methanylylidene))bis(5,6-difluoro-3-oxo-2,3-dihydro-1*H*-indene-2,1-diylidene))dimalononitrile
2PACz	2-(9*H*-carbazol-9-yl)ethyl]phosphonic acid
BFN	1,3,5-tri(*N*-(naphthalene-1-yl)-*N*′-(1,1′-biphenyl-3-yl)-9,9′-dihexyl-2*H*-fluorene-2-yl-amine) benzene
BFSN	1,3,5-tri(*N*-(naphthalene-1-yl)-*N*′-(dibenzothiophene-4-yl)-9,9′-2*H*-dihexylfluorene-2-yl-amine)benzene
BCP	2,9-Dimethyl-4,7-diphenyl-1,10-phenanthroline
P3HT	Poly(3-hexylthiophene-2,5-diyl)
PDBTT-DPP	Poly{2,6′-4,8-di(5-ethylhexylthienyl)benzo[1,2-*b*;3,4-*b*]dithiophene-*alt*-5,5′-dibutyloctyl-3,6-bis(5-thiophen-2-yl)pyrrolo[3,4-*c*]pyrrole-1,4-dione}
PBDTT-SeDPP	Poly{2,6′-4,8-di(5-ethylhexylthienyl)benzo[1,2-*b*;3,4-*b*]dithiophene-*alt*-2,5-bis(2-butyloctyl)-3,6-bis(selenophene-2-yl)pyrrolo[3,4-*c*]pyrrole-1,4-dione}
IEIC	2,2′-[[6,6,12,12-Tetrakis(4-hexylphenyl)-6,12-dihydrodithieno[2′,3′:4,5]-*s*-indaceno[1,2-*b*:5,6-*b*′]dithiophene-2,8-diyl]bis[methylidyne(3-oxo-1*H*-indene-2,1(3*H*)-diylidene)]]bis[propanedinitrile]
IEICO	2,2′-((2*Z*,2′*Z*)-((5,5′-bis(4,4,9,9-tetrakis(4-hexylphenyl)-4,9-dihydro-*s*-indaceno[1,2-*b*:5,6-*b*′]dithiophene-2,7-diyl)bis(4-((2-ethylhexyl)oxy)thiophene-5,2-diyl))bis(methanylylidene))bis-(3-oxo-2,3-dihydro-1*H*-indene-2,1-diylidene))dimalononitrile, 2,2′-[[4,4,9,9-tetrakis(4-hexylphenyl)-4,9-dihydro-*s*-indaceno[1,2-*b*:5,6-*b*′]dithiophene-2,7-diyl]bis[[4-[(2-ethylhexyl)oxy]-5,2-thiophenediyl]-(*Z*)-methylidyne(3-oxo-1*H*-indene-2,1(3*H*)-diylidene)]]bis-propanedinitrile
IEICO-4F	2,2′-((2*Z*,2′*Z*)-(((4,4,9,9-tetrakis(4-hexylphenyl)-4,9-dihydro-sindaceno[1,2-*b*:5,6-*b*′]dithiophene-2,7-diyl)bis(4-((2-ethylhexyl)oxy)thiophene-5,2-diyl))bis(methanylylidene))bis(5,6-difluoro-3-oxo-2,3-dihydro-1*H*-indene-2,1-diylidene))dimalononitrile
PTB7	Poly[[4,8-bis[(2-ethylhexyl)oxy]benzo[1,2-*b*:4,5-*b*′]dithiophene-2,6-diyl][3-fluoro-2-[(2-ethylhexyl)carbonyl]thieno[3,4-*b*]thiophenediyl]]
PBDTTT-C	Poly[(4,8-bis(2-ethylhexyloxy)benzo[1,2-*b*:4,5-*b*′]dithiophene-2,6-diyl)-*alt*-(4-(2-ethylhexyl)-3-fluorothieno[3,4-*b*]thiophene-)-2-carboxylate-2,6-diyl)]
ITCC	3,9-bis(2-methylene-((3-(1,1-dicyanomethylene)-5,6-difluoro-1*H*-indene-1,2(3*H*)-diylidene)))-5,5,11,11-tetrakis(4-hexylphenyl)-dithieno[2,3-*d*:2′,3′-*d*′]-*s*-indaceno[1,2-*b*:5,6-*b*′]dithiophene
IT-M	3,9-bis(2-methylene-((3-(1,1-dicyanomethylene)-6/7-methyl)-indanone))-5,5,11,11-tetrakis(4-hexylphenyl)-dithieno[2,3-*d*:2′,3′-*d*′]-*s*-indaceno[1,2-*b*:5,6-*b*′]dithiophene
IT-4F	3,9-bis(2-methylene-((3-(1,1-dicyanomethylene)-6,7-difluoro)-indanone))-5,5,11,11-tetrakis(4-hexylphenyl)-dithieno[2,3-*d*:2′,3′-*d*′]-*s*-indaceno[1,2-*b*:5,6-*b*′]dithiophene

explored active layer structure in these devices to overcome the limited exciton diffusion challenges from the bilayer heterojunction cell structure. The bulk heterojunction comprises intricate electron donor and acceptor materials that facilitate exciton diffusion and charge transfer to the corresponding electrodes.[58] This review explores how previously studied average visible transmittance (AVT) of donor–acceptor materials can be utilized for precision agriculture. For enhanced perspective, the AVT of common glass windows is greater than 25%.[59] For various active layer blends and thicknesses, the AVT value will change and affect the amount of crop shading and yield.

Initially, a well-studied combination of donor and acceptor materials in OPV systems included P3HT and PCBM molecules (the full names of all organic materials are provided in Table 1), as seen in Fig. 3. However, device performance using PCBM, fullerene molecules, is limited by the weak absorption in the visible and infrared wavelength range.[60] Even after improving the optimal fabrication parameters for these devices, a limited device efficiency of only 5% was reported in 2005.[22] The PCE has improved to 9.35% with the introduction of low-bandgap donor material, PTB7-Th in 2013.[61] The infrared profile of the solar spectrum consists of 52% of the total irradiance, prompting the investigation of near-infrared acceptors for solar energy harvesting devices.[22] In 2015, Zhan *et al.* reported a novel near-infrared acceptor, ITIC, with the efficiency of blends reported to be 6.8%, and further studies demonstrated the potential for these devices to reach 11.4%.[62] However, the AVT of solar cells plays an important role in greenhouse systems and is dependent on active layer thickness. When the thickness of the active layer increases, the device absorption will increase, such that the efficiency will rise until the series resistance and recombination rate is too high. In contrast and in agreement with the Beer–Lambert law, AVT decreases with increasing device thickness, as demonstrated in Fig. 4.

The relationship between active layer thickness and device transmittance in Fig. 4b demonstrates that the thinnest active layer film yields a high transmittance. On the other hand, the device efficiency increases with increased thickness, as shown in Fig. 4c, up to 100 nm. Layers thicker than 100 nm result in decreased efficiency with lower fill factor values, possibly due to increased series resistance or optical effects. On average, the 53 nm thin film produced the highest AVT at a constant Ag electrode thickness, and the thickest film, at 143 nm, resulted in the lowest AVT, as demonstrated in Fig. 4d.[59] As such, the AVT values are significantly affected by film thickness. However, the active layer thickness can vary depending on the absorption coefficient of the active materials. As active materials significantly influence the PCE, their absorption coefficient is also critical for determining the AVT. The PCE and AVT are important for achieving high LUE. Therefore, it is crucial to understand the relationships among active materials, PCE, AVT, and LUE, a few of which are highlighted in Table 2. However, a comprehensive summary can be found in the literature.[65,66]

The transmittance of an OPV is also dependent on other internal device layers, such as the electrodes. Fig. 5 shows the relationship between device performance and AVT for PBDB-T:ITIC devices from the same study with variable Ag electrode thicknesses.[59] Multicomponent electrodes, such as MoO_3/Ag/MoO_3, helped in effective light management for improved performance. As the electrode thickness increased, the current increased, as shown in Fig. 5a. A similar trend was also observed in the external quantum efficiency measurement shown in Fig. 5b. The thicker cathode layers decreased transmittance and the AVT, as shown in Fig. 5c and d.[59] Details on multicomponent electrodes, including their limitations, are discussed in Section 4.

The drive to study other non-fullerene acceptors designed to capture near-infrared spectra then marked the birth of the

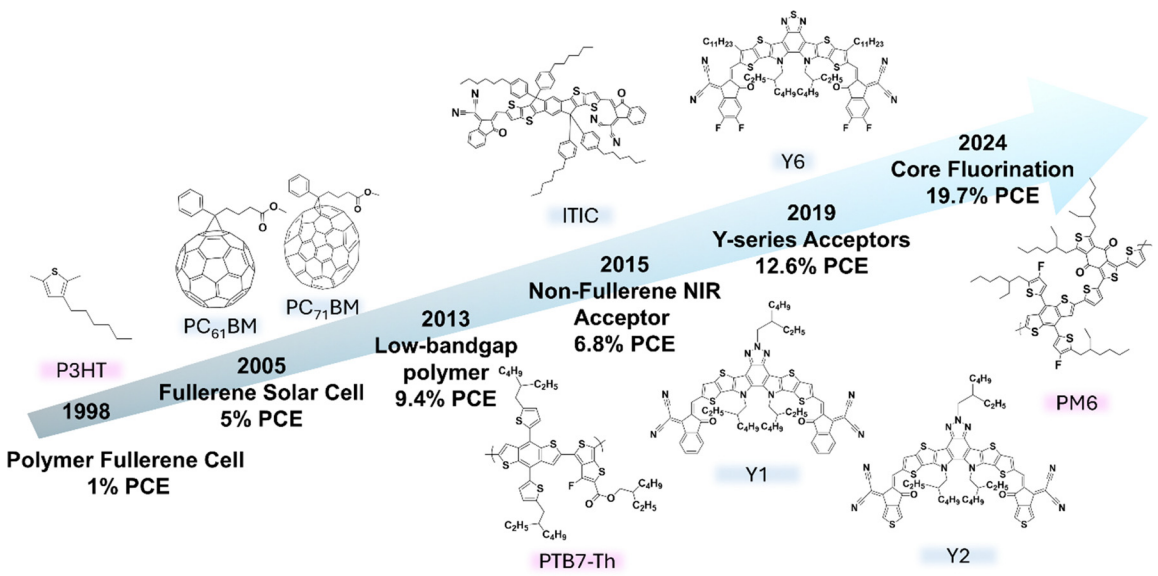

Fig. 3 Timeline of selected donor (pink highlight) and acceptor (blue highlight) workhorse materials discussed in this paper for OPV systems from 1998 to 2024.[22,62–64]

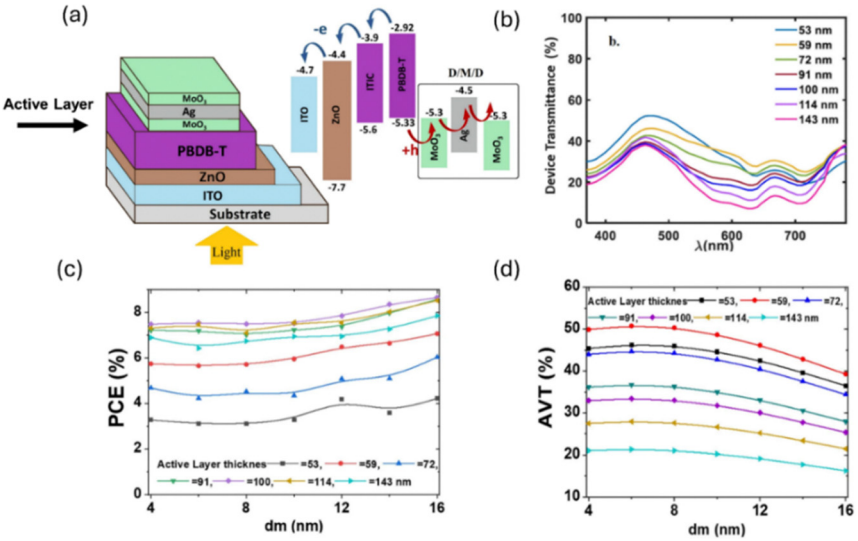

Fig. 4 (a) Device structure and OPV band diagram of ITO/ZnO/PBDB-T:ITIC/MoO_3/Ag/MoO_3. (b) Device transmittance over the visible spectra with varying active layer thickness of t = 53, 59, 72, 91, 100, 114, 143 nm. (c) Power conversion efficiency of various active layer thicknesses relative to varying Ag cathode thicknesses. (d) AVT over the range of active layer thicknesses relative to varying Ag cathode thicknesses. Reproduced with permission.[59] Copyright 2022, Scientific Reports.

Table 2 Some materials composition for ST-OPVs with their PCE, AVT/APT, and LUE values

Active layer	PCE (%)	AVT/APT (%)	LUE (%)	Ref.
PTB7-Th:IUIC	10.2	31.0	3.16	67
PTB7-Th:IHIC	9.8	36.0	3.52	68
PTB7-Th:FOIC	10.3	37.4	3.85	69
PTB7-Th:IEICO-4F	10.0	34.2	3.42	70
PTB7-Th:A078	10.8	45.7	4.94	71
PTB7-Th:H3	8.4	50.1	4.06	27
PM6:Y6	12.9	25.6	3.30	72
PM6:Y6	9.4	42.8	4.02	73
PM6:Y6	13.7	22.2	3.04	74
D18:Y6	12.3	17.0	2.09	75
D18:N3	12.6	22.8	2.87	76
PM6:BTP-eC9:L8-BO	11.4	46.8	5.34	77
PBDB-TF:L8-BO:BTP-eC9	13.0	38.7	5.03	78
PTB7-Th:PBDB-T:PC_{71}BM:ITIC-Th	7.9	63.0	4.98	26

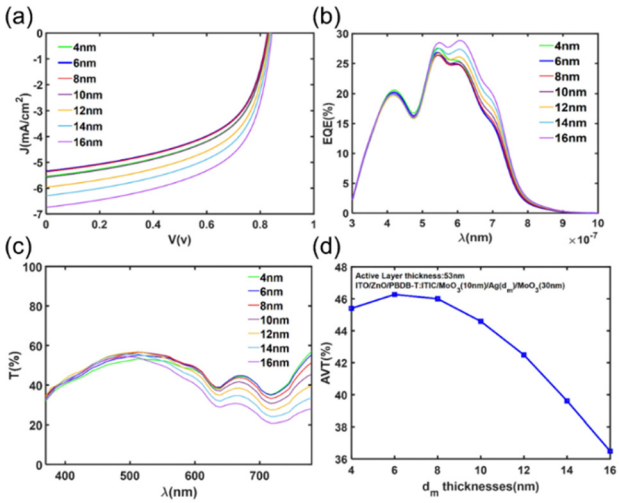

Fig. 5 (a) Performance parameters for the ITO/ZnO/PBDB-T:ITIC/MoO_3/Ag/MoO_3 structure with varying cathode thickness of d = 4, 6, 8, 10, 12, 14, 16 nm. (b) Metal thickness relative to external quantum efficiency. (c) transmission relative to metal thickness. (d) AVT over the range of tested metal thickness. Reproduced with permission.[59] Copyright 2022, Scientific Reports.

Y-series acceptor.[79] To increase the degree of conjugation and enhance molecular charge transfer in ITIC, Yang *et al.* inserted the sp^2-N group, further delocalizing electrons and a redshift in the molecular absorbance seen in Fig. 6a. This discovery enabled the creation of Y1, Y2, and Y6 acceptor molecules. Y6 in OPV devices led to an increased efficiency of 15.7%.[80] In a PM6:Y6 active layer blend, the AVT is 26% and has been shown to increase to 60% at a thickness of 100 nm upon adding a ternary molecule, BFSN, shown in Fig. 6b.[81] This additive led to a reduction in the efficiency of the devices from 12.8% to 11.8%.[81] The broad relationship between efficiency and AVT is shown in Fig. 6(c) amongst many design strategies.

The trade-off in the relationship between AVT and efficiency is calculated in the LUE so that new semitransparent technologies can be compared. One study found that a ternary system with a polymer donor, cyclopentadithiophene, and acceptor has the highest reported near infrared LUE value of 4%.[82] In order to achieve an optimized agrivoltaics system, a high AVT and efficiency in ST-OPV systems must be achieved and further studied for crop use. Fig. 6d demonstrates what an AVT of 30% would look like over a flower specimen. Further plant and device research should report the average photosynthetic transmittance to optimize future agrivoltaic systems.

3.2. Semitransparent PPVs

PPVs are a rapidly advancing technology with improvements in efficiency from 3.8%[83] to over 26%[34,35,84] in recent years. This

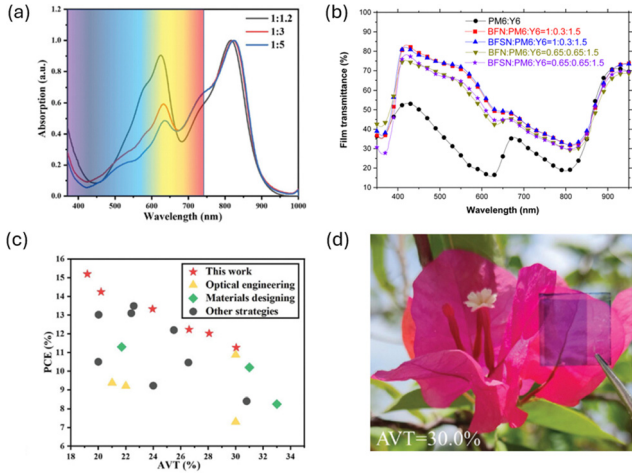

Fig. 6 (a) Normalized absorption spectra of PM6, Y6-BO, and 2PACz demonstrating infrared device absorption. Reproduced with permission.[80] Copyright 2022, Advanced Energy Materials. (b) Percent film transmittance of ITO/PEDOT:PSS/BFSN, PM6, Y6. Reproduced with permission.[81] Copyright 2022, Scientific Reports. (c) The relationship between device architecture and AVT considers optical engineering, materials design, other strategies, and the work presented by Jing *et al.*[80] (d) Thin film held up next to a flower, demonstrating an AVT of 30%. Reproduced with permission.[80] Copyright 2022, Advanced Energy Materials.

progress is attributed to their intrinsic material properties, such as a high optical absorption coefficient, enhanced carrier mobility, and extensive carrier diffusion length.[85–87] Advanced techniques, including interface engineering, carrier management, and additive engineering, have further influenced the rapid progress.[88,89] The unprecedented growth of PPVs is also associated with their ambient and solution processability at low temperatures below 200 °C.[90–92] This contributes to the economic viability of this groundbreaking PV technology. Furthermore, their solution processability makes PPVs compatible with flexible substrates like polyethylene terephthalate. The crystal structure of perovskites with an ABX_3 formula is illustrated in Fig. 7a, where X is an anion and A and B are cations of differing sizes, with A being larger in radius.[93]

Through the compositional engineering in the structure, the bandgap of perovskite materials can be tuned from 1.2 to 3.5 eV, as shown in Fig. 7b.[94] Through this bandgap engineering, the absorption range of perovskite materials can be adjusted for the application of agrivoltaics for specific species of plants. Like ST-OPVs, PPVs can also be utilized as ST-PPVs by controlling their composition or thickness.[50] A study by Shi *et al.* investigated ST-PPVs using a wide-bandgap perovskite composed of $Cs_{0.2}FA_{0.8}Pb(I_{0.6}Br_{0.4})_3$.[49] The concentration of perovskite was varied from 0.2 M to 1.0 M to obtain different levels of transmittance influenced by varying film thickness. Perovskite films exhibited optimal transparency at lower concentrations, as shown in Fig. 8a. The thicknesses of the perovskite layers corresponding to concentrations of 0.2, 0.4, 0.5, 0.6, 0.8, and 1.0 M are 110, 197, 252, 291, 362 and 440 nm, respectively. The device efficiency increased from 10.2% to 14.8% as thickness increased from 252 nm to 440 nm (efficiencies for devices with 110 nm and 197 nm thickness layers were not obtained). The transmittance spectra of ST-PPVs with a device architecture of ITO/NiOx/perovskite/C_{60}/BCP/ITO are presented in Fig. 8b. The AVT for these perovskite films was calculated over the wavelength range between 400 nm and 800 nm. The introduction of surface modification on NiOx, a hole transport layer, with 2PACz enhanced the alignment of work function within the device. By optimizing the thickness of ITO as a top transparent electrode, a high efficiency of 14.4% was achieved for ST-PPVs, with an AVT of 38%, as depicted in Fig. 8c. From this data, the LUE value is calculated to be ~5.5%, notably higher than other referenced studies.

Yu *et al.* also explored ST-PPVs, focusing on key factors affecting the device performance and stability through the compositional modification of $APbI_xBr_{3-x}$ (A = CsFAMA, CsFA, and MA) perovskites.[95] The influence of modification at A- and X-site within $APbX_3$ perovskites on performance and stability was critically assessed. Fig. 8d demonstrates that the perovskite films showed varying compositions at the A-site and X-site. The abbreviation from A-1 to A-4 indicated an increase in the ratio of Br to I from 0.51 to 1.95. Interestingly, an increase in the Br ratio at the X-site resulted in higher transmittance and a shift in the bandgap from 1.63 to 1.92 eV. ST-PPVs with CsFA-2 perovskite, with a band gap of approximately 1.74 eV, were fabricated with a perovskite layer thickness ranging from 100 nm to 400 nm. The transmittance significantly increased below 700 nm with decreasing thickness, as shown in Fig. 8e. These findings underscore the potential of ST-PPVs in agrivoltaic applications, where high transmittance and device performance

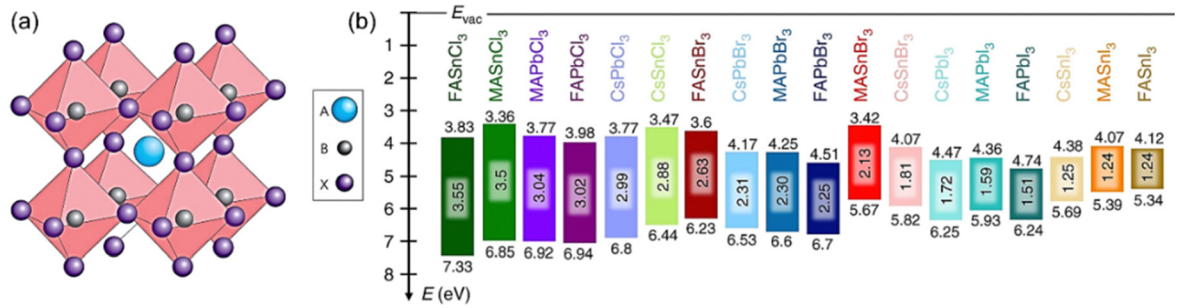

Fig. 7 (a) Cubic perovskite crystal structure. Reproduced with permission.[93] Copyright 2014, Macmillan Publishers Limited. (b) Energy level diagram of the 18 metal halide perovskites. Reproduced with permission.[94] Copyright, Nature Communications.

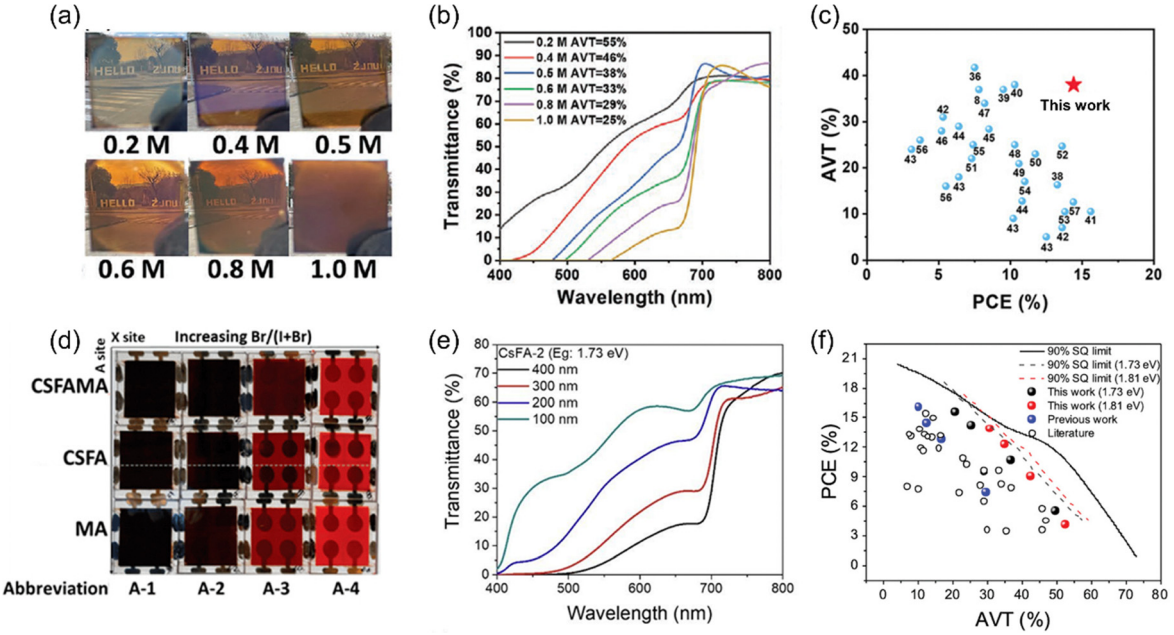

Fig. 8 (a) Perovskite films with different molar concentrations. (b) Transmittance spectra of ST-PSCs with different concentrations. (c) Comparison of AVTs and efficiencies with other works. Reproduced with permission.[49] Copyright 2022, Wiley-VCH GmbH. (d) Perovskite devices with different color tunability through control of the cation such as MA, FA, and Cs and halides such as iodide and bromide compositions. (e) Transmittance spectra of ST-PPVs with different film thicknesses of CsFA-2 film. (f) Efficiencies and AVTs of their previous work and with literature. Reproduced with permission.[95] Copyright 2022, Wiley-VCH GmbH.

are crucial. The trends in efficiency and AVT discussed here, along with other references represented in Fig. 8f, highlight that the LUE value exceeds 4%, demonstrating the promising capabilities of ST-PPVs in integrating agricultural and photovoltaic applications effectively.

In Fig. 9a, Yu *et al.* introduced the maximum theoretical LUE value predicted for the perovskite films.[95] The inputs for these LUE calculations for ST-PPVs were estimated using a transfer matrix method and by assuming a voltage at 90% of the value predicted by the Shockley–Queisser limit. Simulation results indicate that the highest LUE value is 5.7%, with an ideal band gap of approximately 2.4 eV and film thicknesses of about 250 nm and above. Meanwhile, the LUE map based on the reported literature showed the highest LUE at around 5.2% with 1.7 eV of bandgap and 200 nm of film thickness, as illustrated in Fig. 9b. However, along with the importance of LUE, the specific absorption wavelength is particularly significant for agrivoltaic applications. This absorption region will be discussed in the following section. Other forms of controlling PPV transparency can be achieved through translucent devices without compromising the efficiency and aesthetics required for platform integration, such as buildings.[96] Various translucent devices, including cells and modules, manufactured with laser-induced micro-patterning demonstrate how new module designs can meet the optical LUE objectives for building integration.[96] This could be potentially further explored for agrivoltaics.

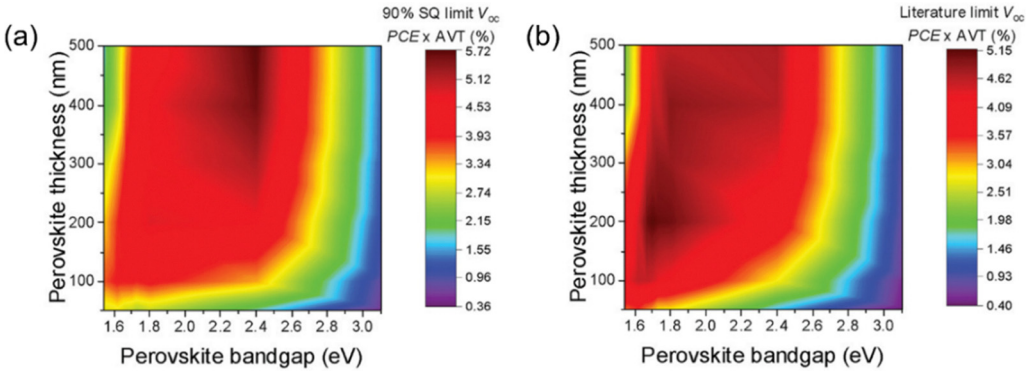

Fig. 9 The maximum theoretical efficiency of ST-PPVs is determined by LUE (PCE × AVT), using efficiency values calculated from (a) V_{oc} at 90% of the Shockley–Queisser limit and (b) the highest Voc related to the band gap reported in the literature. Reproduced with permission.[95] Copyright 2022, Wiley-VCH GmbH.

3.3. Utilizing ST-OPVs and ST-PPVs in agrivoltaic systems

To incorporate ST-OPVs and ST-PPVs into agrivoltaic systems, the known photosynthetic active radiation for the targeted crop species is required. The absorption spectra of major plant photosynthetic pigments and active materials in ST-PVs are depicted in Fig. 10. Each graph highlights the green wavelength range (500–600 nm) for simple visual comparison. On average, single leaves have high absorptivity in the photosynthetic active radiation range (85%) and low absorptivity in the near-infrared (15%). According to Fig. 10a, key pigments such as Chlorophyll A, which is predominant in many plants, absorb primarily in blue and red regions of the spectrum, whereas Chlorophyll B also absorbs these wavelengths but within a narrower range. Plants rich in carotenoids will also absorb blue-green radiation, although minimally.[97]

The light and energy ratios plants are exposed to matter for their ultimate growth. Blue light, for example, is important for early development phases in plants, promoting processes like stomatal opening and stem growth, while red light facilitates flowering and bud formation. Green light exposure has demonstrated a potential increase in leaf growth and biomass production despite plants having low absorption of this wavelength.[102] In nature, green light absorption may also be used in plants as a signaling mechanism for leaf inclination. In addition, early stem elongation, leaf growth, stomatal conductance, and plant biomass are each stimulated by a minimal degree of green light exposure.[103] Considering these requirements, photoactive materials in ST-PVs that absorb the NIR and allow blue and red-light transmission are typically preferred for plant growth. As shown in Fig. 10b and d, organic donor and acceptor materials for ST-OPVs mostly absorb light at a wavelength longer than green, making them suitable for transmitting blue light to the crops. In terms of the red spectrum, donor materials like P3HT, PDBTT-DPP, and PBDTT-SeDPP, and acceptor materials such as IEIC, IEICO, and IEICO-4F, are particularly suitable for agrivoltaics systems as the active material's absorption spectra do not interfere with that of major light-harvesting pigments in plants. Meanwhile, materials such as PTB7, PBDTTT-C, ITCC, ITIC, IT-M, and IT-4F, which absorb in the red regions, could also be effectively utilized. A recent study reported an upscaled PM6:PYTF blend OPV for agrivoltaic application, demonstrating adequate light transmission properties (with AVT between 36 and 45%) and an overview of the observed device degradation from various greenhouse stressors.[104]

For ST-PPVs, the absorption edge can shift with changes in the perovskite composition.[100] For instance, Fig. 10c shows the absorption spectra of $CsPb(I_{1-x}Br_x)_3$ perovskite materials at different bromide to iodine ratios. With values of $x = 0.9$ or 1.0, the absorption edge appears near the green region, shifting towards red as the bromide ratio decreases. Perovskite materials have a broader absorption range than organic materials, exhibiting sharp peaks in specific regions. This versatility benefits their use in PV applications, although it may restrict their suitability in agrivoltaics for diverse plant species.

3.4. Agrivoltaic greenhouse applications: crop shading

As previously stated, the success of ST-OPVs and ST-PPVs depends heavily on the light and thermal requirements of the crop species. Shading has already been explored for various

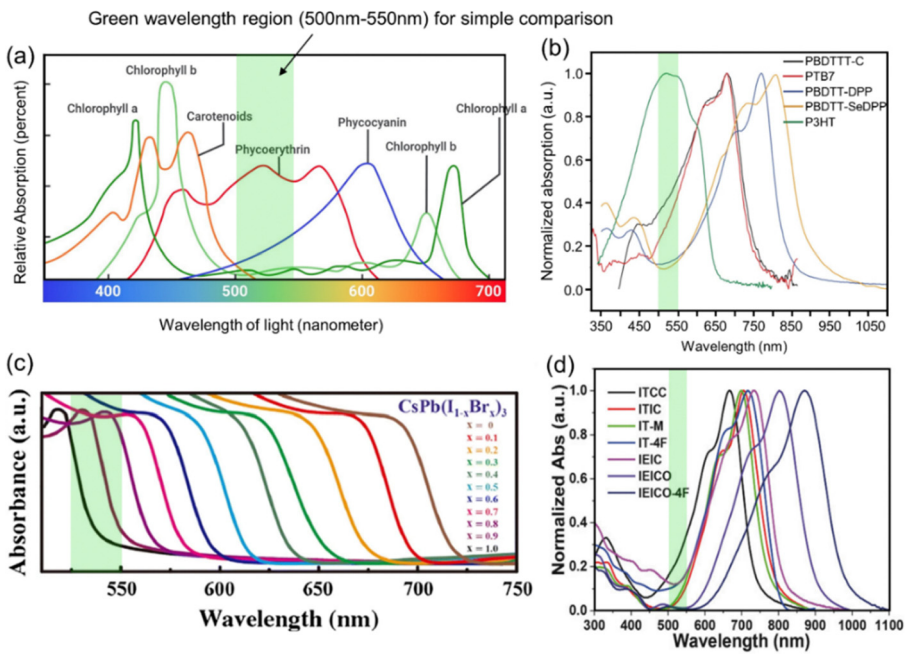

Fig. 10 Absorption spectra of (a) plant photosynthetic pigments. Reproduced with permission.[98] Copyright 2020, CircuitBread, (b) donor materials for ST-OPVs. Reproduced with permission.[99] Copyright 2015, Macmillan Publishers Limited, (c) all inorganic $CsPb(I1\text{-}xBrx)_3$ perovskite for ST-PPVs. Reproduced with permission.[100] Copyright 2020, Springer, and (d) acceptor materials for ST-OPVs. Reproduced with permission.[101] Copyright 2018, WILEY-VCH Verlag GmbH & Co. KGaA, Weinheim.

reasons, such as reducing the crop's evapotranspiration rates to conserve water and lowering the air temperature in the greenhouse to mitigate plant stress.[105–107] This section specifically discusses case studies of integrated ST-PV systems and the partial shading effects in greenhouse structures regarding crop yield across the globe. Other semitransparent systems, such as dye-sensitized solar cells, amorphous silicon, CdTe, *etc.*, have been applied to agrivoltaic systems as well; thus, this section highlights the diversity of ongoing work.[108,109]

One shading study conducted by Cossu *et al.*, based on commercial installations in Sardinia, Italy, discussed the shadowing dynamics in greenhouses using various ratios of opaque silicon PV cover ratios.[110] This study demonstrated that high light-demanding crops such as tomato, sweet pepper, and cucumber reached optimal crop yield with a 25% overhead shading cover ratio. Medium light-demanding species in the same research study found that basil, spinach, strawberry, and lettuce yield also remained consistent below this 25% crop shading threshold, as shown in Fig. 11. Low-light floricultural plants, dracaena, kalanchoe, and poinsettia, also demonstrated high yields across all photovoltaic coverage levels. With a 32–100% crop cover ratio, raspberry, wild strawberry, and blueberry each demonstrated higher antioxidant levels, illustrating one aspect of the nutritional value that shading can contribute to precision growth.[110]

In addition, a separate study conducted in Brazil reported that the total dry mass of tomato fruit in a control *versus* a treatment with a 52% shading screen was 550 and 420 g m^{-2}, respectively.[111] However, a case study in Kunming, China, tested monocrystalline silicon ST-PV systems covering over 20% of greenhouse rooftop structures, showing no significant differences in tomato growth.[14] Thus, up to 20 to 25% of the incoming solar radiation could be diverted to electricity without affecting the yield of some horticultural crops.

The integration of ST-OPVs and ST-PPVs as radiation-harvesting layers over greenhouse structures represents a novel approach in agrivoltaic technology. Due to their unique light transmission capabilities, reporting an AVT is essential when performing an agrivoltaic research study. Fig. 12a demonstrates how certain colors may affect crop productivity,[112] while Fig. 12b compares tomato crop height under red *vs.* blue ST-OPV modules.[113] In a pioneering study on agrivoltaic OPV integration, devices with an approximate 20% measured transmissivity covered 37% of the greenhouse roof area while researchers examined microclimate, yield, and physiological parameters.[114] Results showed a higher leaf area index, average

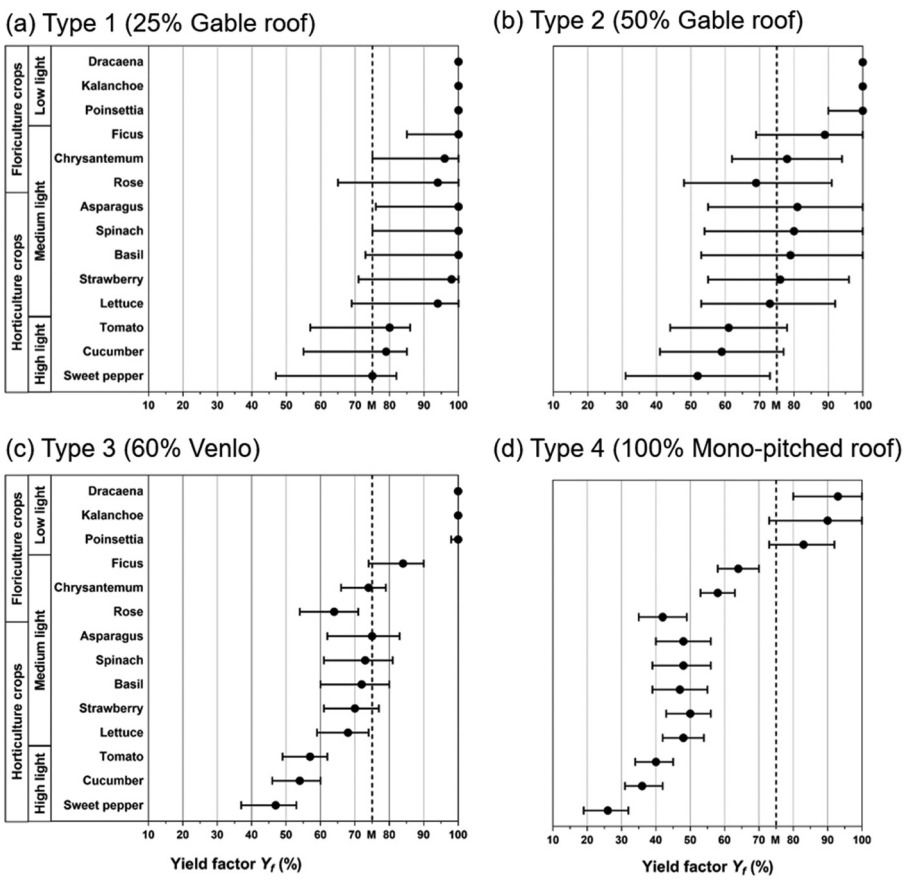

Fig. 11 Comparison of the four silicon PV greenhouse shading types based on total cover ratio, 25%, 50%, 60%, and 100% ((a)–(d) respectively) in Sardinia, Italy *versus* calculated yield according to the plants required daily light integral. The *M* value on each graph represents the minimum acceptable yield factor on a yearly basis. Reproduced with permission.[110] Copyright 2020, ScienceDirect.

fruit mass, and cumulative yield in the OPV system compared to the 25% black-shaded control system, with no significant differences in the following year.[114] The reported AVT spectrum for this module peaked at 475 nm and 720 nm.[115]

Another study using dye-sensitized solar shading (without precise transmissivity data) presented lower early yields, stomatal conductance, and photosynthetic rates for tomato plants but found improved fruit quality, such as increased sugar content.[109] In Kitzingen, Germany, an agrivoltaic research team reported red and blue OPV greenhouse transmittance values of 32.2 and 28.8%, covering 27.3 and 26.8% of the ground area, respectively. Their findings show faster tomato growth under OPV shading, although the accumulated yield was higher in the control system (see Fig. 12b).[113] Furthermore, Gnayem *et al.* compared silicon glass, plastic, and organic solar cells in greenhouses producing cucumbers in Kfar, Israel, and revealed the potential of OPV modules to balance energy production and crop growth.[116]

Precision farming techniques can also use models to predict the overall crop yield or mass and the energy generation under various OPV cover ratios and angles for multiple agrivoltaics systems. In Tucson, AZ, USA, an agrivoltaic model was able to accurately predict lettuce crop shoot weight and estimate the yearly electric energy generated at 8.9 kW h m^{-2} $year^{-1}$ with 25% OPV coverage and a 3.3% efficiency.[117] Scientists found that the developed model predicted that 49% OPV coverage was sufficient to meet the total energy demand of the greenhouse.[117] This kind of predictive modeling is useful for farmers to estimate the energy yield and operational costs of implementing ST-OPV technology over various climate environments. Other methods to assess OPV arrays in greenhouses have been investigated.[118] Future research analyzing the relationship between the AVT of the ST-PV devices and crop yield data needs to be reported to demonstrate the benefits of selective and reliable ST-PV integration into agrivoltaic systems.

4. Limitations of semitransparent PVs

4.1. Stability

Although OPVs and PPVs have seen significant efficiency improvements, long-term stability remains a challenge as they are susceptible to oxidation, high temperature, and their relatively delicate chemical bonds compared to conventional inorganic PVs.[119,120] Therefore, understanding their fundamental degradation mechanism is essential. Different degradation factors include the metastable morphology of the photoactive layer, diffusion of electrodes and buffer layers, oxygen and moisture, illumination, heating, and mechanical stress.[121] For OPVs, the organic materials themselves can degrade through photo-oxidation when exposed to oxygen and sunlight. The bulk heterojunction morphology can also undergo severe phase separation, significantly increasing non-geminate recombination and decreasing efficiency.[122] Furthermore, the interface stability between the active layer, transport layers, and electrodes is also critical, as any of these interfacial degradation mechanisms can reduce the charge carrier mobility and, therefore, the overall efficiency of the device.[123] In the case of PPVs, stability issues are often attributed to the sensitivity of perovskite materials to moisture, heat, and UV radiation.[124] Perovskite can degrade into its constituent components when in contact with moisture, leading to a loss in its absorption properties. Thermal instability can also cause structure changes within the perovskite layer, affecting the electronic properties and leading to efficiency losses.[124] UV stability is another concern, as prolonged exposure can alter the composition of perovskite materials. To solve these stability issues, considerable research is needed on developing stable electrode materials, synthesizing more robust organic and perovskite compounds, and/or enhancing encapsulation techniques.

4.2. Transparency and stability of top electrodes

Another limitation of ST-PVs involves the low transmittance of the top electrodes made from evaporated materials such as

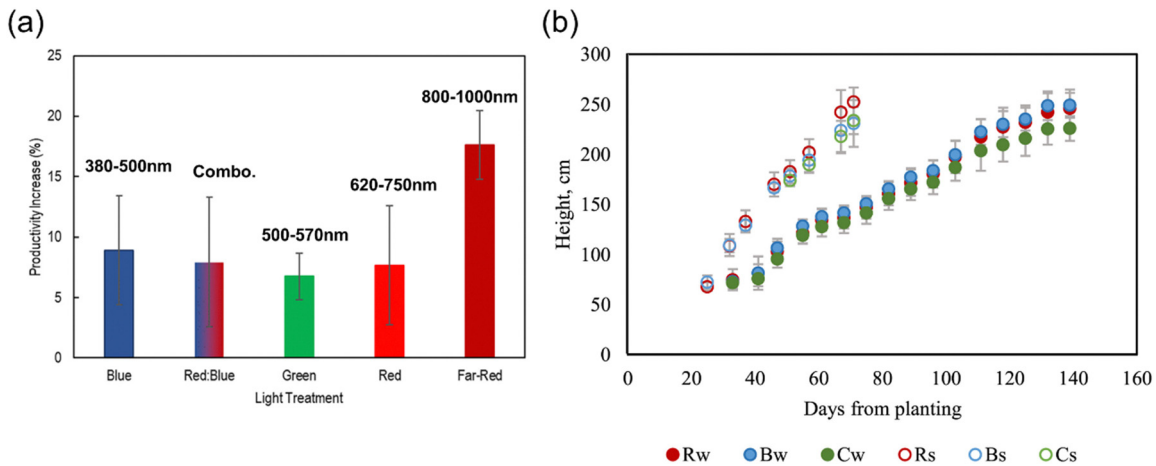

Fig. 12 (a) Productivity increase (mean of leaf area, leaf number, biomass, height) due to changes in LED light quality for horticultural crops (*e.g.*, spinach, rocket, lettuce) from a control "white" light source. Wavelengths were provided as an estimated approximation. Reproduced with permission.[112] Copyright 2023, HortScience. (b) Plant height as a function of days from planting. R, Greenhouse with Red OPV modules; B, Greenhouse with blue OPV modules; C, Control Greenhouse; Subscripts w and s refer to summer and winter seasons. Reproduced with permission.[113] Copyright 2023, ScienceDirect.

aluminum, silver, or gold. To increase their transmittance, the thickness of these electrodes can be reduced. However, this reduction in thickness can significantly increase their electrical resistivity, negatively affecting efficiency. This situation requires considering a trade-off between the electrode thickness and efficiency, similar to the compromise made between the thickness of the active layer and efficiency. As illustrated in Fig. 13a, there is a noticeable drop in transmittance when the electrode thickness exceeds 20 nm.[125] Conversely, the resistivity of a silver electrode begins to increase dramatically when the thickness falls below 10nm, as shown in Fig. 13b.

In practice, a thickness of 25 nm is selected for optimal device performance, achieving an efficiency of 8.4%. Additionally, thinner silver layers are more susceptible to degradation. An oxide-metal-oxide structure is introduced to address this issue, as demonstrated in Fig. 13c.[125] This structural modification has been proven to significantly enhance device stability when exposed to air, unlike devices with only silver, which degrades much faster. This rapid degradation of silver-only electrodes is depicted in Fig. 13d. Although such evolving techniques improve the transparency and stability of the top electrodes, these thermally evaporated top electrodes are still one of the biggest hurdles to their commercialization. Therefore, it is essential to develop an alternative method for the commercialization of fully solution-processable top electrodes.[126–128]

4.3. Solvent toxicity and lead leaching

Device toxicity is also a significant concern, especially for agricultural applications. Solution processing of OPVs and PPVs often uses toxic solvents, including halogenated and aromatic hydrocarbon solvents like chlorobenzene, chloroform, and dimethylformamide. To address this issue, research is intensively focused on environmentally benign solvents for processing OPVs/PPVs, such as 2-methyl-tetrahydrofuran and *N*-methyl-pyrrolidone.[129] One approach to developing eco-friendly solvent-processed OPVs/PPVs is to test alternative solvents for well-established materials. Another widely applied method is modifying the structure of well-established molecules while maintaining key properties like charge transport, molecular packing, absorption coefficient, and carrier mobilities.[130]

Regarding toxicity, potential lead (Pb) leaching from lead-based PPVs is also recognized as a major environmental concern for large-scale commercialization. Pb plays a crucial role in PPVs as an ideal divalent cation with suitable ionic radii and an ideal electronic configuration, such as Pb 6s lone-pair states and Pb 6p orbitals.[131] However, Pb is considered a health hazard and a harmful element for both natural and built environments.[132] Yan *et al.* conducted quantitative research on lead leaching in five benchmark PPVs: $MAPbI_3$, $FA_{0.95}MA_{0.05}Pb(I_{0.95}Br_{0.05})_3$, $Cs_{0.05}(FA_{0.85}MA_{0.15})_{0.95}Pb(I_{0.85}Br_{0.15})_3$, $CsPbI_3$, and $CsPbI_2Br$.[133] Rapid Pb leaching was observed, with more than 60% of the total Pb leaching from the PPVs within the first 120 seconds of aqueous exposure. The Pb leaching process was found to vary depending on the moisture stability, film quality, and total Pb amount in the film. To mitigate this issue, researchers are increasingly focusing on developing Pb-free PPVs and PPVs with reduced amounts of Pb, such as $ASnX_3$ tin perovskites, $A_2B(I)B(III)X_6$ double perovskites, and Sn/Pb mixed perovskites.[134,135] However, Sn-based PPVs, with an efficiency above 14%,[136,137] are significantly behind their Pb-based counterparts and are also unstable. Also, Sn-based PPVs could also be problematic in terms of health and safety. Therefore, it is important to develop new methods to improve both the performance and environmental stability of Pb-free PPV devices to meet IEC qualification standards.[138,139]

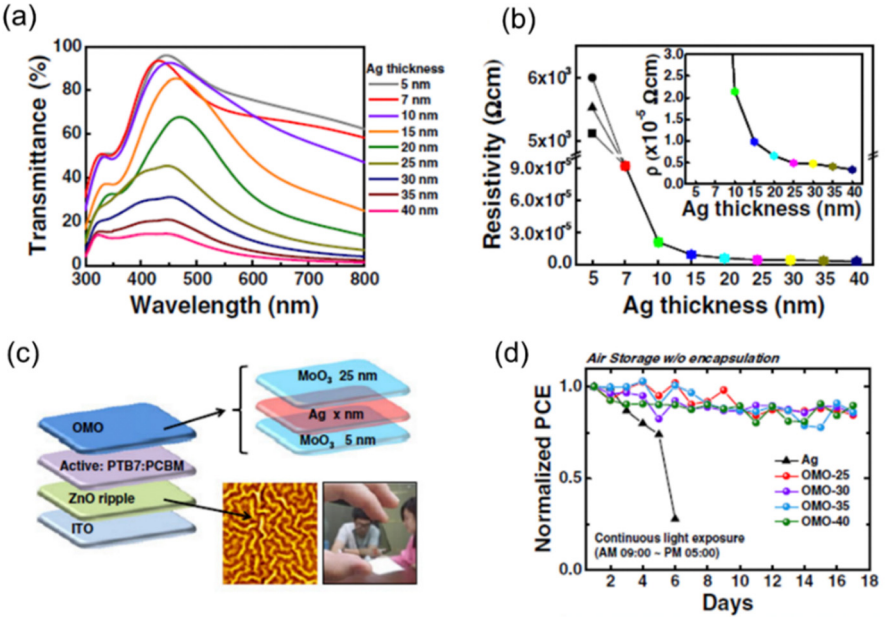

Fig. 13 (a) Transmittance and (b) resistivity of silver electrodes with various thicknesses. (c) Device configuration, and (d) device stability with oxide-metal-oxide structure in air without encapsulation. Reproduced with permission.[125] Copyright, 2017 John Wiley & Sons, Ltd.

Recently, new approaches such as lead chelation and adsorption have been explored to maintain device performance with lead while preventing lead leaching upon damage.[140,141] For instance, Fei *et al.* investigated a lead chelating hole transport layer that can strongly interact with lead ions, resulting in a high PCE of 21.8% for a minimodule with an area of 26.9 cm^2.[142] In addition, Zhang *et al.* introduced lead immobilization methods that transform water-soluble lead ions into insoluble, non-bioavailable, and non-transportable forms over a wide range of pH and temperature conditions.[143] These methods include grain encapsulation, lead complexation, structural integration, and lead adsorption. Combining multiple strategies is suggested to achieve higher lead sequestration efficiencies.

The scientific community is divided about the use of Pb in PPV technologies. There are two schools of thought on the matter. Some judge that the amount of Pb in the conceived potential technology is acceptable. It would be much less than current Pb-based technologies such as lead-acid batteries, solder, cathode-ray tube glass, and waste-printed circuit boards.[144,145] Others consider that PPVs present a danger to people in manufacturing, the environment, and end users. Though this may not be a direct comparison in terms of volumetric content, it is believed that the average amount of lead, for instance, in current lead-acid batteries is about 10 kilograms,[146] which far exceeds the stipulated lead content in PPV panels. For comparison, the amount of lead is estimated to be about 1 gram per 1 m^2 size panel.[147] Thus, in this regard, they believe the Pb content is not significant, especially when PPVs are packaged, sealed, and encapsulated to avoid Pb leaching. For agrivoltaics/greenhouse applications, we side with the second school of thought as the idea of Pb leaching in agricultural environments, which, to any degree, would pose a risk to the health of our communities.

5. Perspective

Although many studies suggest the application of ST-PVs for agrivoltaics, there is still a lack of direct research focused on ST-OPV and ST-PPV agrivoltaic greenhouse integration. The implementation of ST-PVs in agrivoltaics or greenhouse systems is still in its early stages, which provides an opportunity to foster increased agrivoltaic research.

However, semi-transparent luminescent solar concentrator designs have been tested and are ready for greenhouse applications. They have low power conversion efficiencies of 7%.[17,148] Various designs are adapting to new research suggesting that quantum dots, organic dyes, and reflective surface geometries can increase light extraction for improved system performance.[148] Further work into the discussed limitations will soon initiate these advances to become a part of our everyday lives. In the meantime, expanding our library of optimal photosynthetic plant growth conditions under various filters and reporting AVT values can help us narrow down the most desirable systems. Due to the potential toxicity of perovskite materials, as discussed, and issues like microplastic waste, ensuring the health and safety of the agrivoltaic food we consume needs to be a priority. Despite these existing challenges related to OPVs and PPVs, recent advancements in the field have shown promising developments. A noteworthy example is Heliatek's recent success in achieving IEC 61215 ageing certification for the first time in OPV technology for their flexible product, HeliaSol.[149] This industry standard defines the design and qualification of silicon PV modules for long-term operation in open-air, terrestrial applications. This certification is significant as it confirms the durability of flexible OPV, marking it the first commercially available in the HeliaSol series of OPV products to meet such rigorous standards. The certification by TÜV Rheinland underscores Heliatek's technological advancement and boosts confidence in OPVs for more demanding installations globally. For PPVs, they were recently shown to pass the (i) IEC 61215:2016 thermal cycling test for $FAPbI_3$-based cells,[150] (ii) IEC 61215:2016 damp heat and humidity freeze tests for $Cs_{0.05}FA_{0.8}MA_{0.15}Pb(I_{0.85}Br_{0.15})_3$ and $FA_{0.85}MA_{0.15}Pb(I_{0.85}Br_{0.15})_3$-based cells,[151] (iii) IEC 61215:2016 damp heat test, thermal cycling test, and ultraviolet preconditioning test, for $(5\text{-AVA})_xMA_{1-x}PbI_3$ perovskite-based cells, exhibiting over a 9000 hours of operational stability,[152] in a lab environment; and (iv) IEC 61215/61730 at industry level, by Microquanta.[153] With crop yields increasingly affected by climate change, these certifications for OPV and PPV design represent a milestone in potentially meeting the agrivoltaic goals we see in the future.

6. Conclusion

There remains a demand for integrating renewable energy devices into agricultural land use. The unique properties of emerging thin-film semitransparent organic and perovskite photovoltaics, such as transparency and tunability, make them particularly promising for agrivoltaics. For instance, these solar modules can be integrated into greenhouse rooftops, allowing selective light transmission to ensure appropriate wavelengths for plant growth while converting excess light into electricity. This review highlights the potential of integrating ST-PV systems into greenhouse applications with key metrics such as AVT, LUE, and efficiency. Current research indicates that ST-OPVs and -PPVs offer 10–50% of AVT values and efficiencies of around 5–17%. Considering the trade-off between efficiency and AVT, the LUE metric is crucial to demonstrate the potential of these technologies. In summary, LUE values reach 5% for ST-OPVs and 5.5% for ST-PPVs. In comparison, the most efficient luminescent solar concentrator device had a much lower LUE value of only 2.6%.[17] Although seemingly inefficient, luminescent solar concentrator devices can offer much longer stability properties than current OPV or PPV systems, potentially favorable for current dual-land use integration. Although a high LUE value is generally desirable for agrivoltaic applications, it is not always the sole factor, as spectral engineering plays a crucial role in optimizing light absorption for agricultural productivity. In this review, we compared the absorption characteristics of ST-PVs with different photoactive materials and compositions to the absorption spectra of various plant light-absorbing

pigments, such as chlorophyll A, chlorophyll B, and carotenoids. This comparison provides insights into spectral engineering required for agrivoltaic applications tailored to different plant species. In addition, we discussed the current limitations of these techniques, such as stability and toxicity for agricultural applications. Further research in photoactive materials, encapsulation techniques, and compositional engineering is required to integrate ST-PVs into agrivoltaic systems. Investigating crop shading and device performance will soon play a pivotal role in transforming agricultural practices, supporting both clean energy production and sustainable agriculture. The InSPIRE team, supported by the U.S. Department of Energy, has developed an interactive agrivoltaic map and calculator to explore current agrivoltaic projects in the United States and assess the nationwide feasibility.[154] In the future, we look forward to ongoing advancements in ST-OPV and ST-PPV agrivoltaic systems around the world, aiming to benefit a growing society and preserve our natural environment.

Acronyms

OPVs	Organic photovoltaics
PPVs	Perovskite photovoltaics
ST-PVs	Semitransparent photovoltaics
AVT	Average visible transmittance
LUE	Light utilization efficiency (LUE = Device Power Conversion Efficiency (PCE) × AVT)

Data availability

Data sharing is not applicable to this article as no datasets were generated or analysed for the current manuscript.

Conflicts of interest

There are no conflicts to declare.

Acknowledgements

N. R. and E. D. G. acknowledge funding support from the U.S. Department of Defense, Army Research Laboratory, and Army Research Office under grant number W911NF-23-2-0. N. Y. D. acknowledges support from the Materials Research Institute (MRI) and the Institute of Energy and the Environment (IEE) of The Pennsylvania State University, University Park. A. R. K. was supported by the USDA National Institute of Food and Agriculture and Hatch Appropriations under Project #PEN05001 and Accession #7007612.

References

1 U.S. energy consumption increases between 0% and 15% by 2050 - U.S. Energy Information Administration (EIA), **https://www.eia.gov/todayinenergy/detail.php?id=56040**, (accessed June 28, 2024).
2 M. C. Hunter, R. G. Smith, M. E. Schipanski, L. W. Atwood and D. A. Mortensen, *BioScience*, 2017, **67**, 386–391.
3 R. M. Beyer and A. Manica, *Nat. Commun.*, 2020, **11**, 5633.
4 Ocean Acidification, Today and in the Future | NOAA Climate.gov, **https://www.climate.gov/news-features/featured-images/ocean-acidification-today-and-future**, (accessed June 28, 2024).
5 *Living Planet Report 2022 – Building a nature-positive society*, ed. Almond R. E. A., Grooten M., Juffe Bignoli, D. & Petersen, T., WWF, Gland, Switzerland.
6 K. A. Naylor, *UN-Water, Blueprint for acceleration: sustainable development goal 6 synthesis report on water and sanitation*, 2023, United Nations, New York, 2023.
7 *Inventory of U.S. Greenhouse Gas Emissions and Sinks 1990-2022*, U.S. Environmental Protection Agency, EPA 430R-24004, 2024.
8 J. Macknick, H. Hartmann, G. Barron-Gafford, B. Beatty, R. Burton, C. Seok-Choi, M. Davis, R. Davis, J. Figueroa, A. Garrett and L. Hain, *The 5 Cs of Agrivoltaic Success Factors in the United States: Lessons From the InSPIRE Research Study*, National Renewable Energy Laboratory, 2022.
9 S. Sanford, *Reducing greenhouse energy consumption— An overview*, University of Wisconsin-Extenstion, 2011.
10 E. Cuce, D. Harjunowibowo and P. M. Cuce, *Renewable Sustainable Energy Rev.*, 2016, **64**, 34–59.
11 Agrivoltaics: Pairing Solar Power and Agriculture in the Northwest, **https://www.climatehubs.usda.gov/hubs/northwest/topic/agrivoltaics-pairing-solar-power-and-agriculture-northwest**, (accessed June 28, 2024).
12 Brite Solar – Solar Technologies, **https://www.britesolar.com**, (accessed July 29, 2024).
13 S. Sanford, *Reducing greenhouse energy consumption - An overview*, 2011.
14 R. H. EmamHassanien, *Renewable Energy*, 2018, **121**, 377–388.
15 A. M. Detweiler, C. E. Mioni, K. L. Hellier, J. J. Allen, S. A. Carter, B. M. Bebout, E. E. Fleming, C. Corrado and L. E. Prufert-Bebout, *Algal Res.*, 2015, **9**, 170–177.
16 S. M. Lu, S. Amaducci, S. Gorjian, M. Haworth, C. Hägglund, T. Ma, S. Zainali and P. E. Campana, *Joule*, 2024, **8**, 2483–2522.
17 T. Warner, K. P. Ghiggino and G. Rosengarten, *Sol. Energy*, 2022, **246**, 119–140.
18 O. Essahili, M. Ouafi and O. Moudam, *Sol. Energy*, 2022, **245**, 58–66.
19 M. Kaltenbrunner, M. S. White, E. D. Głowacki, T. Sekitani, T. Someya, N. S. Sariciftci and S. Bauer, *Nat. Commun.*, 2012, **3**, 770.
20 C. J. M. Emmott, J. A. Röhr, M. Campoy-Quiles, T. Kirchartz, A. Urbina, N. J. Ekins-Daukes and J. Nelson, *Energy Environ. Sci.*, 2015, **8**, 1317–1328.
21 P. Cheng and Y. Yang, *Acc. Chem. Res.*, 2020, **53**, 1218–1228.
22 D. Meng, R. Zheng, Y. Zhao, E. Zhang, L. Dou and Y. Yang, *Adv. Mater.*, 2022, **34**, 2107330.
23 N. Y. Doumon and L. J. A. Koster, *Solar RRL*, 2019, **3**, 1800301.

24 N. Y. Doumon, F. V. Houard, J. Dong, H. Yao, G. Portale, J. Hou and L. J. A. Koster, *Org. Electron.*, 2019, **69**, 255–262.
25 N. Y. Doumon, G. Wang, R. C. Chiechi, L. Jan and A. Koster, *J. Mater. Chem. C*, 2017, **5**, 6611.
26 M. Nam, H. Y. Noh, J.-H. Kang, J. Cho, B. K. Min, J. W. Shim and D.-H. Ko, *Nano Energy*, 2019, **58**, 652–659.
27 Y. Li, C. He, L. Zuo, F. Zhao, L. Zhan, X. Li, R. Xia, H.-L. Yip, C.-Z. Li, X. Liu and H. Chen, *Adv. Energy Mater.*, 2021, **11**, 2003408.
28 W. Gao, Q. An, R. Ming, D. Xie, K. Wu, Z. Luo, Y. Zou, F. Zhang and C. Yang, *Adv. Funct. Mater.*, 2017, **1702194**, 1–10.
29 J. Hou, M. Park, S. Zhang, Y. Yao, L.-M. Chen, J.-H. Li and Y. Yang, *Macromolecules*, 2008, **41**, 6012–6018.
30 C. Zuo, H. J. Bolink, H. Han, J. Huang, D. Cahen and L. Ding, *Adv. Sci.*, 2016, **3**, 1500324.
31 J. Wang, Z. Zheng, P. Bi, Z. Chen, Y. Wang, X. Liu, S. Zhang, X. Hao, M. Zhang, Y. Li and J. Hou, *Natl. Sci. Rev.*, 2023, **10**, nwad085.
32 Z. Zheng, J. Wang, P. Bi, J. Ren, Y. Wang, Y. Yang, X. Liu, S. Zhang and J. Hou, *Joule*, 2022, **6**, 171–184.
33 Z. Chen, J. Ge, W. Song, X. Tong, H. Liu, X. Yu, J. Li, J. Shi, L. Xie, C. Han, Q. Liu and Z. Ge, *Adv. Mater.*, 2024, **36**, 2406690.
34 C. Liu, Y. Yang, H. Chen, J. Xu, A. Liu, A. S. R. Bati, H. Zhu, L. Grater, S. S. Hadke, C. Huang, V. K. Sangwan, T. Cai, D. Shin, L. X. Chen, M. C. Hersam, C. A. Mirkin, B. Chen, M. G. Kanatzidis and E. H. Sargent, *Science*, 2023, **382**, 810–815.
35 J. Park, J. Kim, H.-S. Yun, M. J. Paik, E. Noh, H. J. Mun, M. G. Kim, T. J. Shin and S. I. Seok, *Nature*, 2023, **616**, 724–730.
36 S.-H. Lim, H.-J. Seok, M.-J. Kwak, D.-H. Choi, S.-K. Kim, D.-H. Kim and H.-K. Kim, *Nano Energy*, 2021, **82**, 105703.
37 Y. Zhu, L. Shu and Z. Fan, *Chem. Res. Chin. Univ.*, 2020, **36**, 366–376.
38 J. Sun and J. J. Jasieniak, *J. Phys. D: Appl. Phys.*, 2017, **50**, 093001.
39 H. Lee, S. Jeong, J.-H. Kim, Y.-R. Jo, H. J. Eun, B. Park, S. C. Yoon, J. H. Kim, S.-H. Lee and S. Park, *npj Flexible Electron.*, 2023, **7**, 1–9.
40 O. Kruse, J. Rupprecht, J. H. Mussgnug, G. C. Dismukes and B. Hankamer, *Photochem. Photobiol. Sci.*, 2005, **4**, 957–970.
41 E. J. Stallknecht, C. K. Herrera, C. Yang, I. King, T. D. Sharkey, R. R. Lunt and E. S. Runkle, *Sci. Rep.*, 2023, **13**, 1903.
42 H.-W. Cheng, Y. Zhao and Y. Yang, *Adv. Energy Mater.*, 2022, **12**, 2102908.
43 R. E. Blankenship, *Molecular Mechanisms of Photosynthesis*, John Wiley & Sons, 2021.
44 X.-G. Zhu, S. P. Long and D. R. Ort, *Curr. Opin. Biotechnol*, 2008, **19**, 153–159.
45 L. La Notte, L. Giordano, E. Calabrò, R. Bedini, G. Colla, G. Puglisi and A. Reale, *Appl. Energy*, 2020, **278**, 115582.
46 R. Waller, M. Kacira, E. Magadley, M. Teitel and I. Yehia, *Agronomy*, 2021, **11**, 1152.
47 C. J. Traverse, R. Pandey, M. C. Barr and R. R. Lunt, *Nat. Energy*, 2017, **2**, 849–860.
48 K. J. McCree, *Agric. Meteorol.*, 1971, **9**, 191–216.
49 H. Shi, L. Zhang, H. Huang, X. Wang, Z. Li, D. Xuan, C. Wang, Y. Ou, C. Ni, D. Li, D. Chi and S. Huang, *Small*, 2022, **18**, 2202144.
50 Z. Yuan, M. Zhang, Z. Yen, M. Feng, X. Jin, A. Ibrahim, M. G. Ahmed, T. Salim, R. A. Gonçalves, T. C. Sum, Y. M. Lam and L. H. Wong, *ACS Appl. Mater. Interfaces*, 2023, **15**, 37629–37639.
51 E. Kondolot Solak and E. Irmak, *RSC Adv.*, 2023, **13**, 12244–12269.
52 K. N'Konou, S. Y. Kim and N. Y. Doumon, *Carbon Energy*, 2024, e579.
53 F. Machui, M. Hösel, N. Li, G. D. Spyropoulos, T. Ameri, R. R. Søndergaard, M. Jørgensen, A. Scheel, D. Gaiser, K. Kreul, D. Lenssen, M. Legros, N. Lemaitre, M. Vilkman, M. Välimäki, S. Nordman, C. J. Brabec and F. C. Krebs, *Energy Environ. Sci.*, 2014, **7**, 2792–2802.
54 C.-S. Tsao, C.-M. Chuang, H.-C. Cha, Y.-Y. Huang, Y.-M. Sung, T.-Y. Chung, Y.-T. Chang, Z.-C. Hu, T.-C. Liu, W.-Y. Ma, Y.-H. Wang, K.-P. Chang, Y.-C. Chao and H.-F. Meng, *Mater. Today Energy*, 2023, **36**, 101340.
55 X. Ru, M. Yang, S. Yin, Y. Wang, C. Hong, F. Peng, Y. Yuan, C. Sun, C. Xue, M. Qu, J. Wang, J. Lu, L. Fang, H. Deng, T. Xie, S. (Frank) Liu, Z. Li and X. Xu, *Joule*, 2024, **8**, 1092–1104.
56 A. M. Oni, A. S. M. Mohsin, Md. M. Rahman and M. B. Hossain Bhuian, *Energy Rep.*, 2024, **11**, 3345–3366.
57 X. Liu, B. P. Rand and S. R. Forrest, *TRECHEM*, 2019, **1**, 815–829.
58 S. Rafique, S. M. Abdullah, K. Sulaiman and M. Iwamoto, *Renewable Sustainable Energy Rev.*, 2017, **84**, 43–53.
59 E. A. Milani, M. Piralaee, S. Ahmadi and A. Asgari, *Sci. Rep.*, 2022, **12**, 14928.
60 S. Cook, H. Ohkita, Y. Kim, J. J. Benson-Smith, D. D. C. Bradley and J. R. Durrant, *Chem. Phys. Lett.*, 2007, **445**, 276–280.
61 S.-H. Liao, H.-J. Jhuo, Y.-S. Cheng and S.-A. Chen, *Adv. Mater.*, 2013, **25**, 4766–4771.
62 Y. Lin, J. Wang, Z.-G. Zhang, H. Bai, Y. Li, D. Zhu and X. Zhan, *Adv. Mater.*, 2015, **27**, 1170–1174.
63 C. J. Brabec, F. Padinger, J. C. Hummelen, R. A. J. Janssen and N. S. Sariciftci, *Synth. Met.*, 1999, **102**, 861–864.
64 K. Liu, Y. Jiang, G. Ran, F. Liu, W. Zhang and X. Zhu, *Joule*, 2024, **8**, 835–851.
65 Y.-W. Su, C.-E. Tsai, T.-C. Liao and K.-H. Wei, *Solar RRL*, 2024, **8**, 2300927.
66 Z. Wu, H. Yin, G. Li and Z. Ji, *Org. Electron.*, 2024, **129**, 107060.
67 B. Jia, S. Dai, Z. Ke, C. Yan, W. Ma and X. Zhan, *Chem. Mater.*, 2018, **30**, 239–245.
68 W. Wang, C. Yan, T.-K. Lau, J. Wang, K. Liu, Y. Fan, X. Lu and X. Zhan, *Adv. Mater.*, 2017, **29**, 1701308.
69 J. Yuan, Y. Zhang, L. Zhou, G. Zhang, H.-L. Yip, T.-K. Lau, X. Lu, C. Zhu, H. Peng, P. A. Johnson, M. Leclerc, Y. Cao, J. Ulanski, Y. Li and Y. Zou, *Joule*, 2019, **3**, 1140–1151.

70 Y. Liu, P. Cheng, T. Li, R. Wang, Y. Li, S.-Y. Chang, Y. Zhu, H.-W. Cheng, K.-H. Wei, X. Zhan, B. Sun and Y. Yang, *ACS Nano*, 2019, **13**, 1071–1077.
71 Y. Li, X. Guo, Z. Peng, B. Qu, H. Yan, H. Ade, M. Zhang and S. R. Forrest, *Proc. Natl. Acad. Sci. U. S. A.*, 2020, **117**, 21147–21154.
72 Y. Bai, C. Zhao, X. Chen, S. Zhang, S. Zhang, T. Hayat, A. Alsaedi, Z. Tan, J. Hou and Y. Li, *J. Mater. Chem. A*, 2019, **7**, 15887–15894.
73 H. I. Jeong, S. Biswas, S. C. Yoon, S.-J. Ko, H. Kim and H. Choi, *Adv. Energy Mater.*, 2021, **11**, 2102397.
74 Y. Zhao, P. Cheng, H. Yang, M. Wang, D. Meng, Y. Zhu, R. Zheng, T. Li, A. Zhang, S. Tan, T. Huang, J. Bian, X. Zhan, P. S. Weiss and Y. Yang, *ACS Nano*, 2022, **16**, 1231–1238.
75 B. Chang, Y.-C. Lin, S. Tan, C.-H. Chen, H.-W. Cheng, Y. Zhao, H.-C. Wang, Q. Xing, L.-Y. Chen, C.-A. Hsieh, C.-Y. Hsiao, Y. Yang and K.-H. Wei, *ACS Appl. Energy Mater.*, 2022, **5**, 13763–13772.
76 C. Xu, K. Jin, Z. Xiao, Z. Zhao, Y. Yan, X. Zhu, X. Li, Z. Zhou, S. Y. Jeong, L. Ding, H. Y. Woo, G. Yuan and F. Zhang, *Solar RRL*, 2022, **6**, 2200308.
77 X. Liu, Z. Zhong, R. Zhu, J. Yu and G. Li, *Joule*, 2022, **6**, 1918–1930.
78 S. Guan, Y. Li, K. Yan, W. Fu, L. Zuo and H. Chen, *Adv. Mater.*, 2022, **34**, 2205844.
79 M. A. Sandri, J. L. Andriolo, M. Witter and T. Dal Ross, *Hortic. Bras.*, 2003, **21**, 642–645.
80 J. Jing, S. Dong, K. Zhang, Z. Zhou, Q. Xue, Y. Song, Z. Du, M. Ren and F. Huang, *Adv. Energy Mater.*, 2022, **12**, 2200453.
81 M. Yan, P. J. Skabara and H. Meng, *J. Mater. Chem. C*, 2023, **11**, 8480–8485.
82 M. F. Albab, M. Jahandar, Y. H. Kim, Y.-K. Kim, M. Shin, A. Prasetio, S. Kim and D. C. Lim, *Nano Energy*, 2024, **121**, 109219.
83 A. Kojima, K. Teshima, Y. Shirai and T. Miyasaka, *J. Am. Chem. Soc.*, 2009, **131**, 6050–6051.
84 Z.-R. Lan, Y.-D. Wang, J.-Y. Shao, D.-X. Ma, Z. Liu, D. Li, Y. Hou, J. Yao and Y.-W. Zhong, *Adv. Funct. Mater.*, 2024, **34**, 2312426.
85 Q. Dong, Y. Fang, Y. Shao, P. Mulligan, J. Qiu, L. Cao and J. Huang, *Science*, 2015, **347**, 967–970.
86 S. De Wolf, J. Holovsky, S.-J. Moon, P. Löper, B. Niesen, M. Ledinsky, F.-J. Haug, J.-H. Yum and C. Ballif, *J. Phys. Chem. Lett.*, 2014, **5**, 1035–1039.
87 Y. Zhao, A. M. Nardes and K. Zhu, *J. Phys. Chem. Lett.*, 2014, **5**, 490–494.
88 J. J. Yoo, G. Seo, M. R. Chua, T. G. Park, Y. Lu, F. Rotermund, Y.-K. Kim, C. S. Moon, N. J. Jeon, J.-P. Correa-Baena, V. Bulović, S. S. Shin, M. G. Bawendi and J. Seo, *Nature*, 2021, **590**, 587–593.
89 J. Jeong, M. Kim, J. Seo, H. Lu, P. Ahlawat, A. Mishra, Y. Yang, M. A. Hope, F. T. Eickemeyer, M. Kim, Y. J. Yoon, I. W. Choi, B. P. Darwich, S. J. Choi, Y. Jo, J. H. Lee, B. Walker, S. M. Zakeeruddin, L. Emsley, U. Rothlisberger, A. Hagfeldt, D. S. Kim, M. Grätzel and J. Y. Kim, *Nature*, 2021, **592**, 381–385.
90 I. M. Asuo, D. Gedamu, N. Y. Doumon, I. Ka, A. Pignolet, S. G. Cloutier and R. Nechache, *Mater. Adv.*, 2020, **1**, 1866–1876.
91 I. M. Asuo, I. Ka, D. Gedamu, A. Pignolet, R. Nechache and S. G. Cloutier, *Sol. Energy Mater. Sol. Cells*, 2019, **200**, 110029.
92 I. M. Asuo, A. M. Varposhti, E. D. Gomez and N. Y. Doumon, *J. Mater. Chem. C*, 2024, **12**, 7562–7571.
93 M. A. Green, A. Ho-Baillie and H. J. Snaith, *Nat. Photonics*, 2014, **8**, 506–514.
94 S. Tao, I. Schmidt, G. Brocks, J. Jiang, I. Tranca, K. Meerholz and S. Olthof, *Nat. Commun.*, 2019, **10**, 2560.
95 J. C. Yu, B. Li, C. J. Dunn, J. Yan, B. T. Diroll, A. S. R. Chesman and J. J. Jasieniak, *Adv. Sci.*, 2022, **9**, 2201487.
96 D. B. Ritzer, B. A. Nejand, M. A. Ruiz-Preciado, S. Gharibzadeh, H. Hu, A. Diercks, T. Feeney, B. S. Richards, T. Abzieher and U. W. Paetzold, *Energy Environ. Sci.*, 2023, **16**, 2212–2225.
97 E. Dănilă and D. D. Lucache, *2016 International Conference and Exposition on Electrical and Power Engineering (EPE)*, 2016, 439–444.
98 How are LEDs used for growing plants?, **https://www.circuitbread.com/ee-faq/how-are-leds-used-for-growing-plants**, (accessed July 3, 2024).
99 Y. (Michael) Yang, W. Chen, L. Dou, W.-H. Chang, H.-S. Duan, B. Bob, G. Li and Y. Yang, *Nat. Photonics*, 2015, **9**, 190–198.
100 T. Ma, S. Wang, Y. Zhang, K. Zhang and L. Yi, *J. Mater. Sci.*, 2020, **55**, 464–479.
101 R. Yu, H. Yao and J. Hou, *Adv. Energy Mater.*, 2018, **8**, 1702814.
102 A. Trivellini, S. Toscano, D. Romano and A. Ferrante, *Plants*, 2023, **12**, 2026.
103 K. M. Folta and S. A. Maruhnich, *J. Exp. Bot.*, 2007, **58**, 3099–3111.
104 X. Rodríguez-Martínez, S. Riera-Galindo, L. E. Aguirre, M. Campoy-Quiles, H. Arwin and O. Inganäs, *Adv. Funct. Mater.*, 2023, **33**, 2213220.
105 B. B. Lin, *Agric. Meteorol.*, 2010, **150**, 510–518.
106 H. A. Ahemd, A. A. Al-Faraj and A. M. Abdel-Ghany, *Sci. Hortic.*, 2016, **201**, 36–45.
107 M. Möller and S. Assouline, *Irrig. Sci.*, 2007, **25**, 171–181.
108 R. H. E. Hassanien, M. Li and F. Yin, *Renewable Energy*, 2018, **121**, 377–388.
109 G. K. Ntinas, K. Kadoglidou, N. Tsivelika, K. Krommydas, A. Kalivas, P. Ralli and M. Irakli, *Horticulturae*, 2019, **5**, 42.
110 M. Cossu, A. Yano, S. Solinas, P. A. Deligios, M. T. Tiloca, A. Cossu and L. Ledda, *Eur. J. Agron.*, 2020, **118**, 126074.
111 M. A. Sandri, J. L. Andriolo, M. Witter and T. Dal Ross, *Hortic. Bras.*, 2003, **21**, 642–645.
112 J. D. Stamford, J. Stevens, P. M. Mullineaux and T. Lawson, *HortScience*, 2023, **52**, 180–196.
113 M. Teitel, R. Grimberg, S. Ozer, H. Vitoshkin, I. Yehia, E. Magadley, A. Levi, E. Ziffer, S. Gantz and A. Levy, *Biosyst. Eng.*, 2023, **232**, 81–96.

114 M. Friman-Peretz, S. Ozer, F. Geoola, E. Magadley, I. Yehia, A. Levi, R. Brikman, S. Gantz, A. Levy, M. Kacira and M. Teitel, *Biosyst. Eng.*, 2020, **197**, 12–31.
115 M. Friman Peretz, F. Geoola, I. Yehia, S. Ozer, A. Levi, E. Magadley, R. Brikman, L. Rosenfeld, A. Levy, M. Kacira and M. Teitel, *Biosyst. Eng.*, 2019, **184**, 24–36.
116 N. Gnayem, E. Magadley, A. Haj-Yahya, S. Masalha, R. Kabha, A. Abasi, H. Barhom, M. Matar, M. Attrash and I. Yehia, *Biosyst. Eng.*, 2024, **241**, 83–94.
117 K. Okada, I. Yehia, M. Teitel and M. Kacira, *Acta Hortic.*, 2018, **1227**, 231–239.
118 R. Waller, M. Kacira, E. Magadley, M. Teitel and I. Yehia, *AgriEngineering*, 2022, **4**, 969–992.
119 S. Y. Kim, C. C. F. Kumachang and N. Y. Doumon, *Solar RRL*, 2023, **7**, 2300155.
120 Y. Zhao, Z. Li, C. Deger, M. Wang, M. Peric, Y. Yin, D. Meng, W. Yang, X. Wang, Q. Xing, B. Chang, E. G. Scott, Y. Zhou, E. Zhang, R. Zheng, J. Bian, Y. Shi, I. Yavuz, K.-H. Wei, K. N. Houk and Y. Yang, *Nat. Sustainable*, 2023, **6**, 539–548.
121 L. Duan and A. Uddin, *Adv. Sci.*, 2020, **7**, 1903259.
122 C. J. Schaffer, C. M. Palumbiny, M. A. Niedermeier, C. Jendrzejewski, G. Santoro, S. V. Roth and P. Müller-Buschbaum, *Adv. Mater.*, 2013, **25**, 6760–6764.
123 A. Turak, *RSC Adv.*, 2013, **3**, 6188–6225.
124 D. Wang, M. Wright, N. K. Elumalai and A. Uddin, *Sol. Energy Mater. Sol. Cells*, 2016, **147**, 255–275.
125 D. C. Lim, J. H. Jeong, K. Hong, S. Nho, J.-Y. Lee, Q. V. Hoang, S. K. Lee, K. Pyo, D. Lee and S. Cho, *Prog. Photovoltaics Res. Appl.*, 2018, **26**, 188–195.
126 L. Sun, W. Zeng, C. Xie, L. Hu, X. Dong, F. Qin, W. Wang, T. Liu, X. Jiang, Y. Jiang and Y. Zhou, *Adv. Mater.*, 2020, **32**, 1907840.
127 D.-S. Leem, A. Edwards, M. Faist, J. Nelson, D. D. C. Bradley and J. C. de Mello, *Adv. Mater.*, 2011, **23**, 4371–4375.
128 A. Kim, Y. Won, K. Woo, S. Jeong and J. Moon, *Adv. Funct. Mater.*, 2014, **24**, 2462–2471.
129 S. Lee, D. Jeong, C. Kim, C. Lee, H. Kang, H. Y. Woo and B. J. Kim, *ACS Nano*, 2020, **14**, 14493–14527.
130 F. Campana, C. Kim, A. Marrocchi and L. Vaccaro, *J. Mater. Chem. C*, 2020, **8**, 15027–15047.
131 Y.-T. Huang, S. R. Kavanagh, D. O. Scanlon, A. Walsh and R. L. Z. Hoye, *Nanotechnology*, 2021, **32**, 132004.
132 A. Babayigit, A. Ethirajan, M. Muller and B. Conings, *Nat. Mater.*, 2016, **15**, 247–251.
133 D. Yan, X. Lu, S. Zhao, Z. Zhang, M. Lu, J. Feng, J. Zhang, K. Spencer, T. Watson, M. Li, B. Hou, F. Wang and Z. Li, *Solar RRL*, 2022, **6**, 2200332.
134 F. Gu, Z. Zhao, C. Wang, H. Rao, B. Zhao, Z. Liu, Z. Bian and C. Huang, *Solar RRL*, 2019, **3**, 1900213.
135 L. Gollino and T. Pauporté, *Solar RRL*, 2021, **5**, 2000616.
136 L. Wang, M. Chen, S. Yang, N. Uezono, Q. Miao, G. Kapil, A. K. Baranwal, Y. Sanehira, D. Wang, D. Liu, T. Ma, K. Ozawa, T. Sakurai, Z. Zhang, Q. Shen and S. Hayase, *ACS Energy Lett.*, 2022, **7**, 3703–3708.
137 L. Wang, Q. Miao, D. Wang, M. Chen, H. Bi, J. Liu, A. K. Baranwal, G. Kapil, Y. Sanehira, T. Kitamura, T. Ma, Z. Zhang, Q. Shen and S. Hayase, *Angew. Chem., Int. Ed.*, 2023, **62**, e202307228.
138 A. Mei, Y. Sheng, Y. Ming, Y. Hu, Y. Rong, W. Zhang, S. Luo, G. Na, C. Tian, X. Hou, Y. Xiong, Z. Zhang, S. Liu, S. Uchida, T.-W. Kim, Y. Yuan, L. Zhang, Y. Zhou and H. Han, *Joule*, 2020, **4**, 2646–2660.
139 M. L. Rencheck, C. Libby, A. Montgomery and J. S. Stein, *Sol. Energy*, 2024, **269**, 112337.
140 X. Li, F. Zhang, H. He, J. J. Berry, K. Zhu and T. Xu, *Nature*, 2020, **578**, 555–558.
141 G. Liu, Y. Zhong, W. Feng, M. Yang, G. Yang, J.-X. Zhong, T. Tian, J.-B. Luo, J. Tao, S. Yang, X.-D. Wang, L. Tan, Y. Chen and W.-Q. Wu, *Angew. Chem., Int. Ed.*, 2022, **61**, e202209464.
142 C. Fei, N. Li, M. Wang, X. Wang, H. Gu, B. Chen, Z. Zhang, Z. Ni, H. Jiao, W. Xu, Z. Shi, Y. Yan and J. Huang, *Science*, 2023, **380**, 823–829.
143 H. Zhang, J.-W. Lee, G. Nasti, R. Handy, A. Abate, M. Grätzel and N.-G. Park, *Nature*, 2023, **617**, 687–695.
144 Y.-M. Li, Y. Wang, M.-J. Chen, T.-Y. Huang, F.-H. Yang and Z.-J. Wang, *Int. J. Environ. Sci. Technol.*, 2023, **20**, 1037–1052.
145 M. S. Rahmanifar, *Electrochim. Acta*, 2017, **235**, 10–18.
146 U. N. Environment, Used Lead Acid Batteries (ULAB) - Waste Lead Acid Batteries (WLAB), **https://www.unep.org/topics/chemicals-and-pollution-action/pollution-and-health/heavy-metals/used-lead-acid-batteries**, (accessed July 15, 2024).
147 B. Chen, C. Fei, S. Chen, H. Gu, X. Xiao and J. Huang, *Nat. Commun.*, 2021, **12**, 5859.
148 L. Shen and X. Yin, *Nano Convergence*, 2022, **9**, 36.
149 Heliatek achieves ICE 61215 certification for lightweight and flexible HeliaSol solar film, **https://ope-journal.com/news/heliatek-achieves-ice-61215-certification-for-lightweight-and-flexible-heliasol-solar-film**, (accessed July 15, 2024).
150 L. Shi, T. L. Young, J. Kim, Y. Sheng, L. Wang, Y. Chen, Z. Feng, M. J. Keevers, X. Hao, P. J. Verlinden, M. A. Green and A. W. Y. Ho-Baillie, *ACS Appl. Mater. Interfaces*, 2017, **9**, 25073–25081.
151 L. Shi, M. P. Bucknall, T. L. Young, M. Zhang, L. Hu, J. Bing, D. S. Lee, J. Kim, T. Wu, N. Takamure, D. R. McKenzie, S. Huang, M. A. Green and A. W. Y. Ho-Baillie, *Science*, 2020, **368**, eaba2412.
152 A. Mei, Y. Sheng, Y. Ming, Y. Hu, Y. Rong, W. Zhang, S. Luo, G. Na, C. Tian, X. Hou, Y. Xiong, Z. Zhang, S. Liu, S. Uchida, T.-W. Kim, Y. Yuan, L. Zhang, Y. Zhou and H. Han, *Joule*, 2020, **4**, 2646–2660.
153 L. Zhang, Y. Wang, X. Meng, J. Zhang, P. Wu, M. Wang, F. Cao, C. Chen, Z. Wang, F. Yang, X. Li, Y. Zou, X. Jin, Y. Jiang, H. Li, Y. Liu, T. Bu, B. Yan, Y. Li, J. Fang, L. Xiao, J. Yang, F. Huang, S. Liu, J. Yao, L. Liao, L. Li, F. Zhang, Y. Zhan, Y. Chen, Y. Mai and L. Ding, *Mater. Futures*, 2024, **3**, 022101.
154 Agrivoltaics Map, **https://openei.org/wiki/InSPIRE/Agrivoltaics_Map**, (accessed July 15, 2024).